

AD-A238 638



2

# NAVAL POSTGRADUATE SCHOOL

## Monterey, California



DTIC  
ELECTE  
JUL 17 1991  
S B D

### THESIS

CONTROL OF FLOW OVER A BACKWARD  
FACING STEP

by

Scott G. Woolman

September 1990

Thesis Advisor:

J. Val Healey

Approved for public release; distribution is unlimited

91-04992



UNCLASSIFIED

SECURITY CLASSIFICATION OF THIS PAGE

REPORT DOCUMENTATION PAGE				Form Approved OMB No 0704-0188	
1a REPORT SECURITY CLASSIFICATION <b>UNCLASSIFIED</b>			1b RESTRICTIVE MARKINGS		
2a SECURITY CLASSIFICATION AUTHORITY			3 DISTRIBUTION/AVAILABILITY OF REPORT  <b>Approved for public release; distribution is unlimited</b>		
2b DECLASSIFICATION/DOWNGRADING SCHEDULE					
4 PERFORMING ORGANIZATION REPORT NUMBER(S)			5 MONITORING ORGANIZATION REPORT NUMBER(S)		
6a NAME OF PERFORMING ORGANIZATION  <b>Naval Postgraduate School</b>		6b OFFICE SYMBOL (if applicable)  <b>Code 67</b>	7a NAME OF MONITORING ORGANIZATION  <b>Naval Postgraduate School</b>		
6c ADDRESS (City, State, and ZIP Code)  <b>Monterey, California 93943-5000</b>			7b ADDRESS (City, State, and ZIP Code)  <b>Monterey, California 93943-5000</b>		
8a NAME OF FUNDING/SPONSORING ORGANIZATION		8b OFFICE SYMBOL (if applicable)	9 PROCUREMENT INSTRUMENT IDENTIFICATION NUMBER		
8c ADDRESS (City, State, and ZIP Code)			10 SOURCE OF FUNDING NUMBERS		
			PROGRAM ELEMENT NO	PROJECT NO	TASK NO
					WORK UNIT ACCESSION NO
11 TITLE (Include Security Classification)  <b>CONTROL OF FLOW OVER A BACKWARD FACING STEP</b>					
12 PERSONAL AUTHOR(S) <b>Woolman, Scott G.</b>					
13a TYPE OF REPORT <b>Master's Thesis</b>		13b TIME COVERED FROM _____ TO _____		14 DATE OF REPORT (Year, Month, Day) <b>1990, September</b>	
				15 PAGE COUNT <b>92</b>	
16 SUPPLEMENTARY NOTATION <b>The views expressed in this thesis are those of the author and do not reflect the official policy or position of the Department of Defense or the U.S. Government.</b>					
17 COSATI CODES			18 SUBJECT TERMS (Continue on reverse if necessary and identify by block number)		
FIELD	GROUP	SUB-GROUP	<b>Backward Facing Step; Bluff-Body Aerodynamics; Flow Tailoring; Blade Strike; Operating Envelopes</b>		
19 ABSTRACT (Continue on reverse if necessary and identify by block number)  <b>The poor aerodynamic design of the superstructures of today's Navy ships create a highly turbulent airwake that can make shipboard helicopter operations quite hazardous. This study is part of a longer-term project to tailor airflow over a ship's helicopter deck in order to improve the poor quality of the airflow. This airflow is thought to be largely responsible for several costly blade strike mishaps involving H-46 helicopters during start-up and shut-down. Numerous computer simulations were conducted using the "Phoenix" Computational Fluid Dynamics code to simulate airflow over a backward-facing-step. The latter represents a simple 2-d model of flow behind a typical hangar/flight deck combination. In each run a deflector of different size, orientation or porosity was placed in a specific location in an attempt to reduce the size of the recirculation zone, the velocities and the turbulence levels. Of the studies</b>					
20 DISTRIBUTION/AVAILABILITY OF ABSTRACT <input checked="" type="checkbox"/> UNCLASSIFIED/UNLIMITED <input type="checkbox"/> SAME AS RPT <input type="checkbox"/> DTIC USERS			21 ABSTRACT SECURITY CLASSIFICATION <b>Unclassified</b>		
22a NAME OF RESPONSIBLE INDIVIDUAL <b>Prof. J. Val Healey</b>			22b TELEPHONE (Include Area Code) <b>(408) 646-2804</b>		22c OFFICE SYMBOL <b>Code 67He</b>

DD Form 1473, JUN 86

Previous editions are obsolete

S/N 0102-LF-014-6603

SECURITY CLASSIFICATION OF THIS PAGE

UNCLASSIFIED

UNCLASSIFIED

SECURITY CLASSIFICATION OF THIS PAGE

#19 - ABSTRACT - (CONTINUED)

involved, a vertical deflector offset downstream with its lower edge at the top of the step produced the best overall results.

Accession For	
NTIS GRA&I	<input checked="checked" type="checkbox"/>
DTIC TAB	<input type="checkbox"/>
Unannounced	<input type="checkbox"/>
Justification	
By	
Distribution/	
Availability Codes	
Dist	Avail and/or Special
A-1	



Approved for public release; distribution is unlimited

Control of Flow Over a Backward Facing Step

by

Scott G. Woolman  
Lieutenant, United States Coast Guard  
B.S., University of California at Davis, 1979

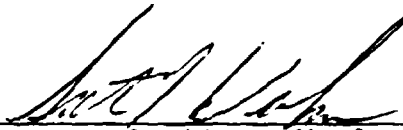
Submitted in partial fulfillment of the  
requirements for the degree of

MASTER OF SCIENCE IN ENGINEERING SCIENCE

from the

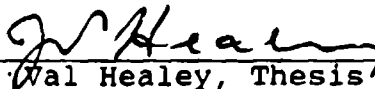
NAVAL POSTGRADUATE SCHOOL  
September 1990

Author:



Scott G. Woolman

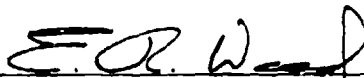
Approved by:



J. Wal Healey, Thesis Advisor



David Salinas, Second Reader



E.R. Wood, Chairman  
Department of Aeronautics and Astronautics

### ABSTRACT

The poor aerodynamic design of the superstructures of today's Navy ships create a highly turbulent airwake that can make shipboard helicopter operations quite hazardous. This study is part of a longer-term project to tailor airflow over a ship's helicopter deck in order to improve the poor quality of the airflow. This airflow is thought to be largely responsible for several costly blade strike mishaps involving H-46 helicopters during start-up and shut-down. Numerous computer simulations were conducted using the "Phoenix" Computational Fluid Dynamics code to simulate airflow over a backward-facing-step. The latter represents a simple 2-d model of flow behind a typical hangar/flight deck combination. In each run a deflector of different size, orientation or porosity was placed in a specific location in an attempt to reduce the size of the recirculation zone, the velocities and the turbulence levels. Of the studies involved, a vertical deflector offset downstream with its lower edge at the top of the step produced the best overall results.

## TABLE OF CONTENTS

I.	INTRODUCTION -----	1
II.	BACKGROUND -----	4
	A. HELICOPTER OPERATIONS -----	4
	B. BLUFF BODY AERODYNAMICS -----	9
	C. FLOW OVER A BACKWARD FACING STEP -----	15
	D. FLOW OVER A TWO-DIMENSIONAL OBSTACLE -----	20
	E. FLOW MODIFICATION -----	22
III.	CFD PROGRAM SETUP -----	27
	A. BACKGROUND -----	27
	B. HOW "PHOENICS" WORKS -----	28
	C. PROBLEM CONFIGURATION -----	31
IV.	RESULTS AND DISCUSSION -----	38
	A. BACKWARD FACING STEP -----	39
	B. TWO-DIMENSIONAL FENCE -----	41
	C. VERTICAL DEFLECTOR ABOVE STEP -----	45
	D. VERTICAL DEFLECTOR OFFSET 12.5MM -----	45
	E. VERTICAL DEFLECTOR OFFSET 25MM -----	48
	F. VERTICAL DEFLECTOR OFFSET 50MM -----	52
	G. SLANTED OFFSET DEFLECTORS -----	56
V.	CONCLUSIONS AND RECOMMENDATIONS -----	66
	APPENDIX: SAMPLE Q1 FILE -----	68
	LIST OF REFERENCES -----	77
	INITIAL DISTRIBUTION LIST -----	80

## LIST OF TABLES

1. FLOW SIMULATION INPUTS -----	32
2. DEFLECTOR CONFIGURATION. -----	36

## LIST OF FIGURES

1.	AOR Class Ship -----	2
2.	Generic Operating Envelope -----	7
3.	Daytime Operating Envelope for BB-63 -----	8
4.	Flow Over Flight Deck -----	10
5.	Mean Streamline Patterns About a Bluff Body -----	11
6.	Separation Cavities for 2-d Flow -----	13
7.	Centerline Streamline Patterns for Flow Reattaching to Top -----	14
8.	Centerline Streamline Patterns for Flow Not Reattaching to Top -----	14
9.	Wake of Hangar--DD-963 -----	16
10.	Backward-facing Step Flowfield -----	17
11.	Reattachment-length Measurements Showing Dependence on the State of the Separating Boundary Layer -----	17
12.	Flow Structure Over 2-d Fence -----	21
13.	Mean Streamlines at a Medium Dense and a Dense Windbreak -----	24
14.	The Wind Speed Reduction of Different Windbreaks ( $H$ = Height of Windbreak) -----	25
15.	Cell Depiction -----	29
16.	Step with Vertical Deflector -----	35
17.	Step with Slanted Deflector -----	37
18.	Backward-Facing-Step -----	40
19.	2-d Fence; 0.0% Porosity -----	42
20.	2-d Fence; 10% Porosity -----	43



21.	2-d Fence; 20% Porosity -----	44
22.	50mm Vertical Deflector; 15% Porosity, 25mm Vertical Gap -----	46
23.	50mm Vertical Deflector; 0.0% Porosity, 12.5mm Vertical Gap -----	47
24.	50mm Vertical Deflector; 15% Porosity, 12.5mm Vertical Gap, 12.5mm Offset Downstream ----	49
25.	50mm Vertical Deflector; 0.0% Porosity, 0.0mm Vertical Gap, 12.5mm Offset Downstream -----	50
26.	50mm Vertical Deflector; 5% Porosity, 12.5mm Vertical Gap, 25mm Offset Downstream -----	51
27.	25mm Vertical Deflector; 0.0% Porosity, 0.0mm Vertical Gap, 50mm Offset Downstream -----	53
28.	50mm Vertical Deflector; 0.0% Porosity, 0.0mm Vertical Gap, 50mm Offset Downstream -----	54
29.	50mm Vertical Deflector; 5% Porosity, 0.0mm Vertical Gap, 50mm Offset Downstream -----	55
30.	50mm Vertical Deflector; 15% Porosity, Bottom Edge -25mm Below Step Top, 50mm Offset Downstream -----	57
31.	50mm Deflector Slanted 30 Degrees; 0.0% Porosity, Bottom Edge 30mm Offset Downstream -----	58
32.	50mm Deflector Slanted 30 Degrees; 10% Porosity, Bottom Edge 30mm Offset Downstream -----	60
33.	50mm Deflector Slanted 30 Degrees; 0.0% Porosity, Bottom Edge 30mm Offset Downstream -----	61
34.	50mm Deflector Slanted 30 Degrees; 5% Porosity, Bottom Edge 50mm Offset Downstream -----	62
35.	50mm Cranked Deflector; 30/60 Degree, 0.0% Porosity, 50mm Offset Downstream -----	63
36.	50mm Cranked Deflector; 45/60 Degree, 0.0% Porosity, 50mm Offset Downstream -----	65

## NOMENCLATURE

BFC	Body Fitted Coordinates
BFS	Backward-Facing-Step
$C_\mu$	Constant in Turbulent Model (= .09)
$C_1$	Constant in Turbulent Model (= 1.44)
$C_2$	Constant in Turbulent Model (= 1.92)
k (or TKE)	Turbulence Kinetic Energy
$u$	Velocity Tensor
$\delta$	Boundary Layer Thickness
$\epsilon$	Rate of Dissipation of Turbulence Energy
$\mu_{eff}$	Effective Dynamic Viscosity
$\sigma_k, \sigma_\epsilon$	Schmidt Numbers for k and $\epsilon$

### ACKNOWLEDGMENTS

A sincere thank you must be given to Professor J. Val Healey. For if it were not for his ever-present patience and sense of optimism this project would still be in the planning stages. For their expertise in computer matters, I would like to thank Mr. Tony Cricelli and Lt. Bill Lonchas.

Lastly, but most importantly, my grateful appreciation goes to my loving family, who supported and generally understood their "grumpy" dad for the last two years.

## I. INTRODUCTION

The Navy's ability to conduct helicopter operations is more important today than ever before. Helicopters are a major contributor to the Antisubmarine and Antisurface Warfare mission areas and are equally important in the role of material supply between fleet ships, both underway and at anchor. The twin rotor helicopter, the H-46, is commonly used in this resupply mission because of its large load carrying ability and tolerance to varying wind conditions while hovering over ships.

The ability of the H-46 to operate in various weather and wind conditions is vital to the smooth and efficient operation of the fleet. However, due to an increasing number of rotor strike mishaps, the overall availability of the H-46 has been reduced. Most of these blade strike mishaps have occurred on AOR, LPA AND LPH type vessels (Figure 1), during rotor engagement or rotor shutdown, with winds of at least moderate strength.

It is generally thought that the main reason for most blade strike mishaps is the turbulent wind conditions encountered on the ship's helicopter deck. The only presently known solution to this problem is a reduction of the rotor engage/disengage envelope. The latter prescribes allowable safe operation limits based on the wind direction and speed.

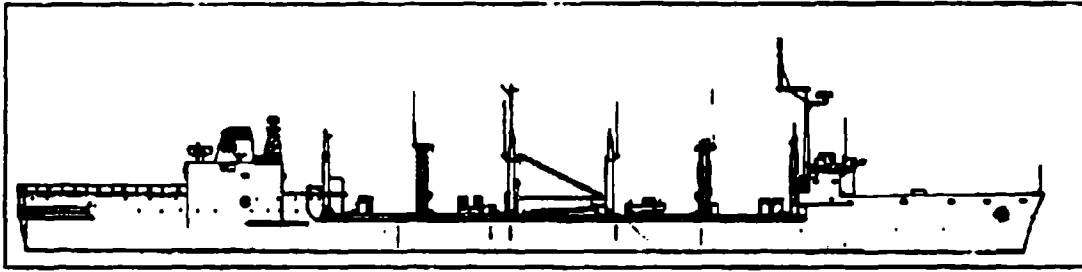


Figure 1. AOR Class Ship [Ref. 1]

The highly turbulent conditions often found on the helicopter deck are a result of the interaction between the wind and the ship's superstructure. When Navy ships were first designed, their mission dependence on helicopters was not foreseen and so little attention was paid to the aerodynamics of the superstructure. Unfortunately, there has been little, if any, improvement in superstructure design, with regards to airflow, on today's newer ships. Thus, the environment around the ships, in which the helicopter must operate, remains quite hazardous.

The Naval Postgraduate School (NPS) has undertaken a series of studies on ship airwake tailoring, with the goal of reducing the level of turbulence and the size of the separated zones on the helicopter deck. This reduction will result in a larger engage/disengage envelope, which in turn, will increase the percentage of time that the H-46 can safely operate. This particular study is the first in a series at NPS to attempt to achieve this goal and will consider only the feasibility of such endeavors by tailoring a two-dimensional

flow over a backward facing step. The "Phoenix" computational fluid dynamics (CFD) code will be utilized to simulate the two-dimensional flow and the tailoring of the airflow will be accomplished in the code with strategically placed deflectors.

First, a more in-depth look at the role of the H-46 in fleet operations will be addressed; this will be followed by a short review of bluff body aerodynamics, ship airwakes, and any wake modification methods used up to the present. After the computer simulations are made, they will be analyzed and recommendations made on step/deflector configurations for the next part of the program, which will be an attempt at experimental verification of the tailoring of two-dimensional flow over a backward facing step in the NPS low speed wind tunnel.

## II. BACKGROUND

### A. HELICOPTER OPERATIONS

Navy fleets, which must travel worldwide, cannot hope to accomplish their mission without the "Mobile Logistic Support Force" (MLSF) ships. [Ref. 2:p. 1.1] This group of ships consists of the following ship classes: AE, AO, AOR, AFS, and AOE. These ships sail with the fleet carrying most of the supplies required for that particular deployment, such as food, fuel, and material goods. There are two basic methods to transfer these supplies from ship to ship, connected replenishment (CONREP) and vertical replenishment (VERTREP). [Ref. 2:p. 1.3]

CONREP is a method that involves two ships steaming side by side within 80 to 200 feet of each other and transferring supplies by means of cables strung between them. This method is commonly used for refueling ships and transferring loads which are too heavy for VERTREP.

The preferred method of replenishment is with helicopters, a method more commonly referred to as VERTREP. Supply items are placed in large cargo nets, lifted by the helicopters, and transferred to the appropriate ships. The specific advantages of VERTREP are:

- (1) Reduction in time required to replenish the supported forces or units.

- (2) Reduction or elimination of time that screening ships are off station.
- (3) Reduction of the number of personnel involved.
- (4) Capability of replenishing units in a dispersed formation.
- (5) Capability of replenishing units engaged in tasks which make it impossible for them to come along side.
- (6) Capability of replenishing units in heavy weather conditions when alongside steaming is hazardous or impossible.
- (7) Capability of replenishing units on station in shallow water or at anchor.

As stated before, the twin rotor H-46 has become the helicopter of choice for this mission and its continuous availability in various weather and wind conditions has become vital in fleet operations. Blade strikes, which are mishaps that occur when a turning rotor blade impacts the helicopter fuselage, cause damage that must be repaired before the helicopter is available again and are numerous enough to threaten a reduction in the safe operating envelope of the H-46.

Though blade strikes typically occur at a very low rotor RPM (usually at the start of rotor engagement or the end of rotor shutdown, when rotor RPM is about 20% of normal), they still pose a significant danger to the aircrews and ground personnel as well as the aircraft. Through the middle of 1989 there have been at least 75 such incidents aboard ships ranging from little or no damage to complete loss of the airframe. The dollar cost can range from just man hour costs



when only inspections are required for a minor strike, to upwards of \$500,000 for a blade strike which involves a sudden stoppage to the drivetrain system. [Ref. 3:p. 4] If the entire airframe is lost, the cost can escalate to well over \$2.7 million, which is the approximate cost of a replacement H-46.

Hidden costs are somewhat harder to measure, but are equally costly. An interruption in the UNREP operation can lead to changes in the entire fleet schedule. This may cause numerous other operations to be changed or canceled to allow the resupply mission to continue.

To avoid blade strikes while operating on shore, or from a ship, the helicopter crews use a chart which is essentially a go/no go chart which tells them if wind direction and speed will allow a safe rotor engagement or disengagement. The generic envelope for the H-46 is shown in Figure 2. There are also ship specific envelopes, an example of which is shown in Figure 3.

These envelopes are developed through dynamic interface testing done by the Naval Air Test Center (NATC). It is a long, laborious, and expensive process which is valid only for the particular combination of ship/helicopter being tested. A description of the testing process is given by Madey and Whitmer [Ref. 5]. Unfortunately, due to the extraordinary variability of wind and sea state conditions, it is nearly impossible to document a completely safe operating envelope.

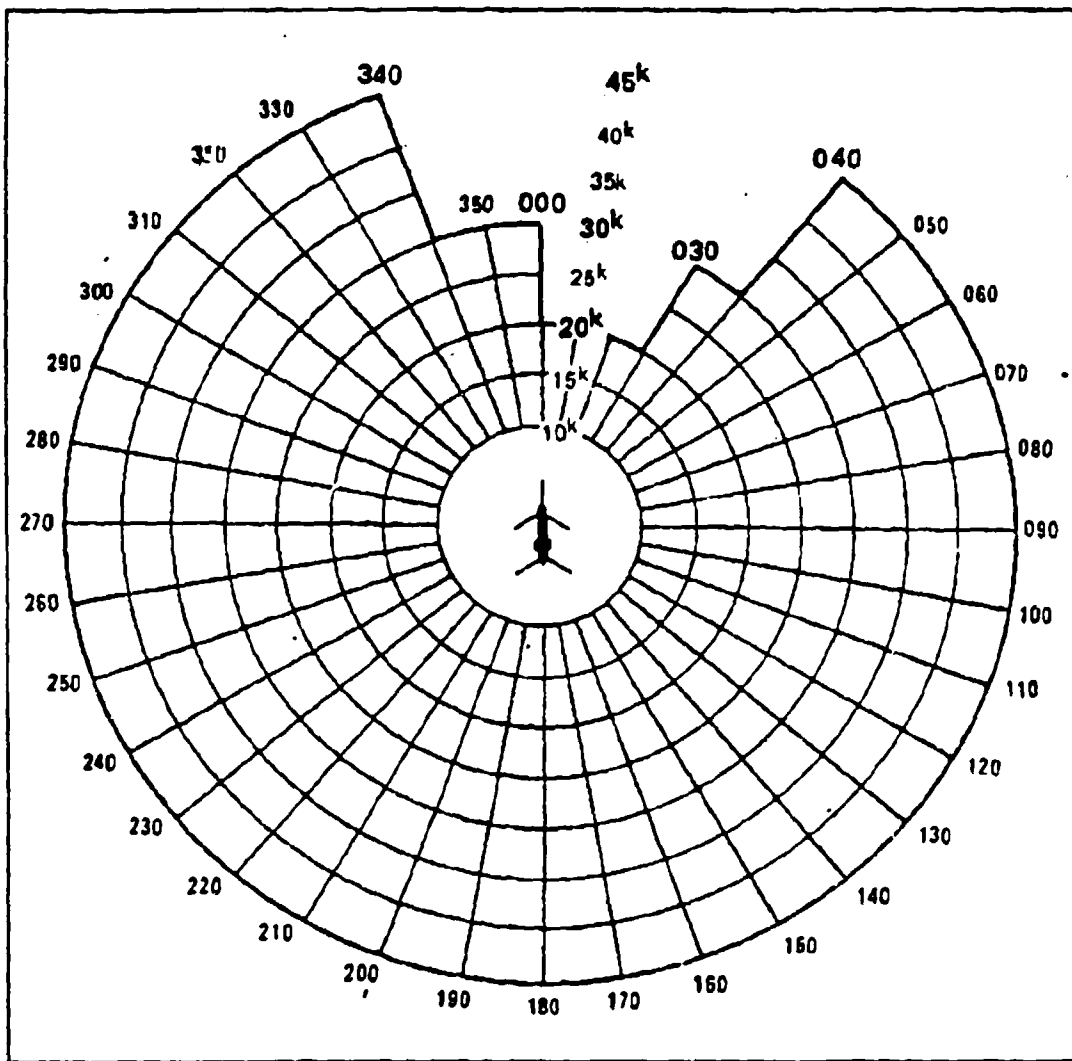


Figure 2. Generic Operating Envelope [Ref. 4]

This is certainly true for the H-46 and the AOR ship combination in which a significant number of the blade strike incidents have occurred while operating inside of the rotor engage/disengage envelope.

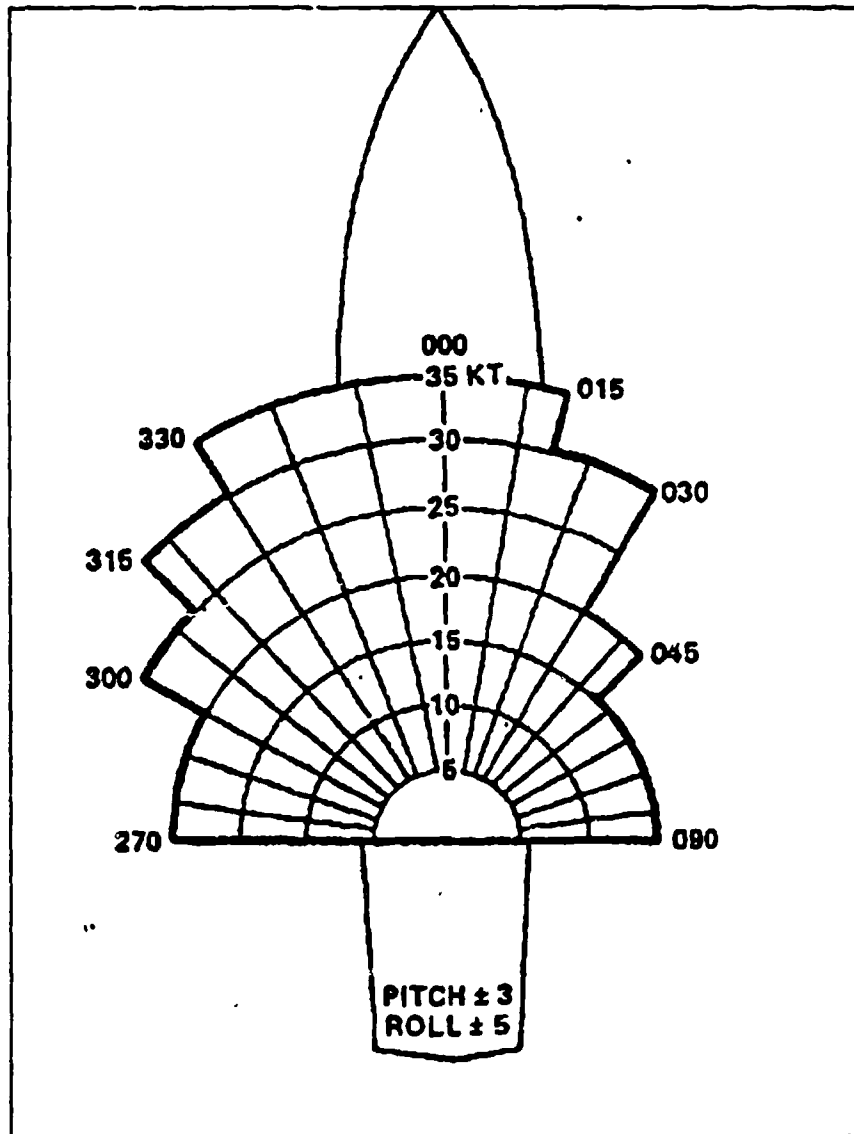


Figure 3. Daytime Operating Envelope for BB-63 [Ref. 4]

This predicament has led to the suggestion that the problem may be solved by simulation [Ref. 6:p. 2]. To achieve this simulation accurately there is a need to predict the freestream airflow over the ship, the ship motion, and the

motion of the helicopter. Healey [Ref. 6:pp. 14-58] looks at what has been done in these fields and lists several other references. The program underway at NPS is attempting to make detailed air-wake maps of model ships for scaling to full-size. So far, visualization of the flow around a model of a DD-963 class destroyer has been completed [Ref. 7] and a similar study of an AOR class ship is presently in progress.

Until that time when a completely accurate rotor engage/disengage envelope is developed, other alternatives must be looked at. This paper explores one such alternative: tailoring the ship airwake in order to reduce the size of the separation zones and the levels of turbulence encountered on the helicopter deck. This approach will not only eventually lead to a safer operating area for the helicopters but, if successful, will increase the size of the rotor engage/disengage envelope, thus allowing the helicopters to operate a greater percentage of time.

#### B. BLUFF BODY AERODYNAMICS

Though the experimental part of this paper will be conducted as a two-dimensional problem, it is an important first step to understanding the three-dimensional airflow experienced by the ship, the helicopter deck, and subsequently the helicopter. Bluff body aerodynamics and their relationship to this problem will first be examined. This is not

meant to be a detailed discourse on the subject, as the references to be cited more than adequately cover the subject.

By definition, a bluff body is one in which, for given flow conditions, there is a massive separated region in its wake. It becomes apparent, after first observing the design of any large class Navy ship (Figure 1) and then a schematic of the observed flow over a model ship (Figure 4), that Navy ships indeed can be considered three-dimensional bluff bodies.

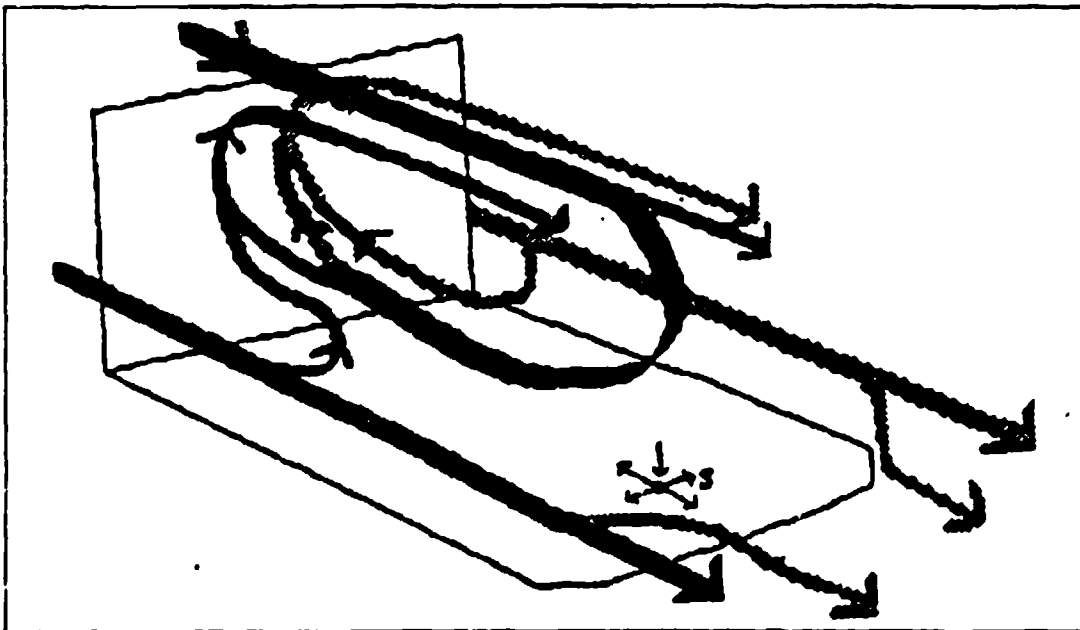


Figure 4. Flow Over Flight Deck [Ref. 7:p. 34]

To start to appreciate the complexity of the flow around a bluff body, one only has to look at a study by Hunt, Abell

Peterka, and Woo. [Ref. 8:pp. 179-200] They detected the presence of an inverted U-shaped vortex, whose ends remained in contact with the ground, on the downwind side of the body and numerous horseshoe vortices that wrap themselves about the upstream base of the body and trail downstream (Figure 5). In addition, turbulence causes the reattachment point to be highly unstable, and alters the flow field around the body by producing increased mixing near the separated shear layers [Ref. 9].

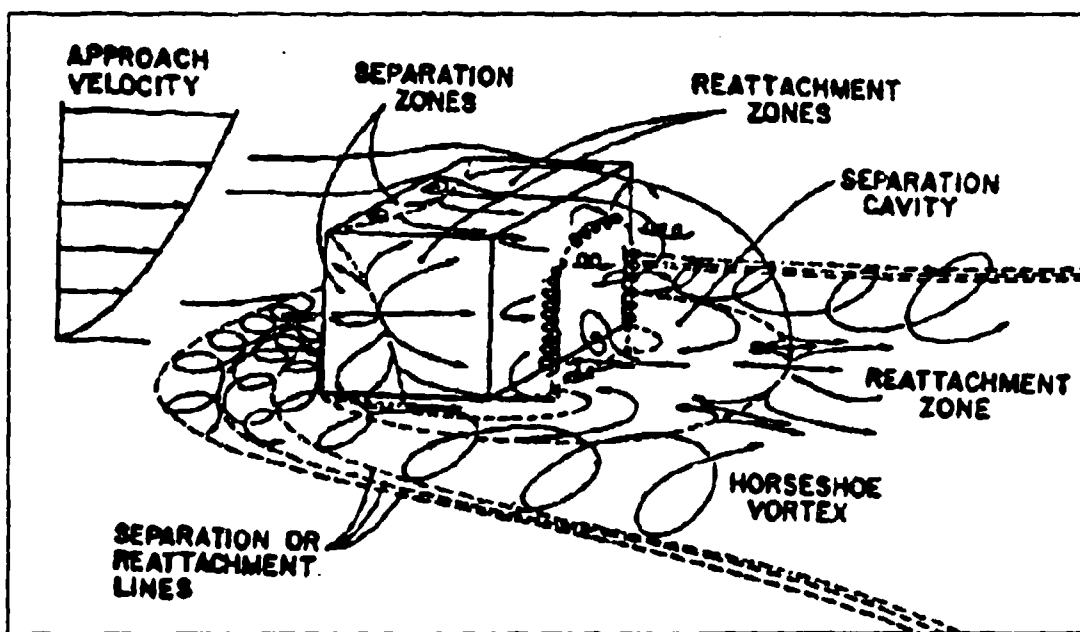


Figure 5. Mean Streamline Patterns About a Bluff Body [Ref. 8]

Trying to relate the flow around a simple bluff body to actual airflow over ships is an extremely difficult task. One can find only few, and then poorly done, studies on the subject. As stated before, the present studies at NPS should rectify that situation soon. Until then, it is necessary to look elsewhere. One such area, where much time and effort have been expended, is in the area of wind flow around buildings and other obstacles [Ref. 10].

Recent investigations in the flow around buildings have advanced the understanding of physical flow processes occurring in the near and far wake region. But, according to Peterka et al. [Ref. 10], even though there has been many studies in this area, there is still a high level of misunderstanding on how the winds actually flow around buildings. They believe that these misconceptions are probably caused by "conceptual extensions of two-dimensional flow". Figure 6 shows the separation zone for a two-dimensional object bounded by streamlines so that the cavities are closed. For a three-dimensional object, these separation lines are no longer valid. Studies which have been conducted in boundary layer wind tunnels [Refs. 11,12] show that three-dimensional objects show fundamental differences in flow patterns relative to those of two-dimensional objects. Since this study is indeed based on two-dimensional flow relating to a three-dimensional problem, it is worthwhile to spend a little time and look at these differences.

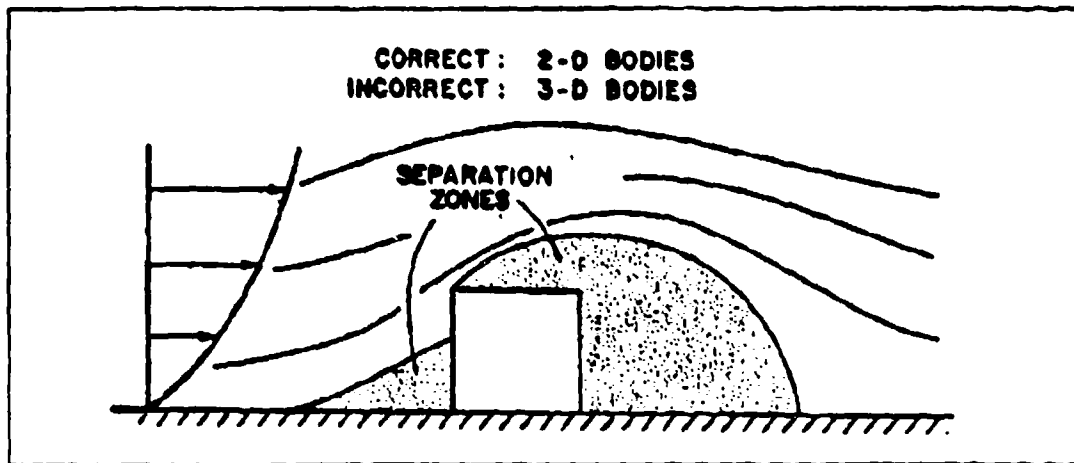


Figure 6. Separation Cavities for 2-d Flow [Ref. 10]

Looking at Figures 7 and 8, the flow approaching the obstacle has separated at some distance upstream, at a point that is dependent, to the first order, on building height-to-width ratio, building height-to-boundary-layer-height ratio and upstream surface roughness [Ref. 10]. The air in this separated flow strikes the building, flows downward and rolls up into a vortex. It then wraps around the building into the horseshoe shape that was discussed before. This horseshoe vortex can be identified in the flow for quite some distance downstream.

The wind that impinges on the front of the building forms a stagnation region somewhere near the top (about  $2/3$  the way up) depending on building height-to-width ratio. [Ref. 10] From this region, flow moves out toward all front edges of the



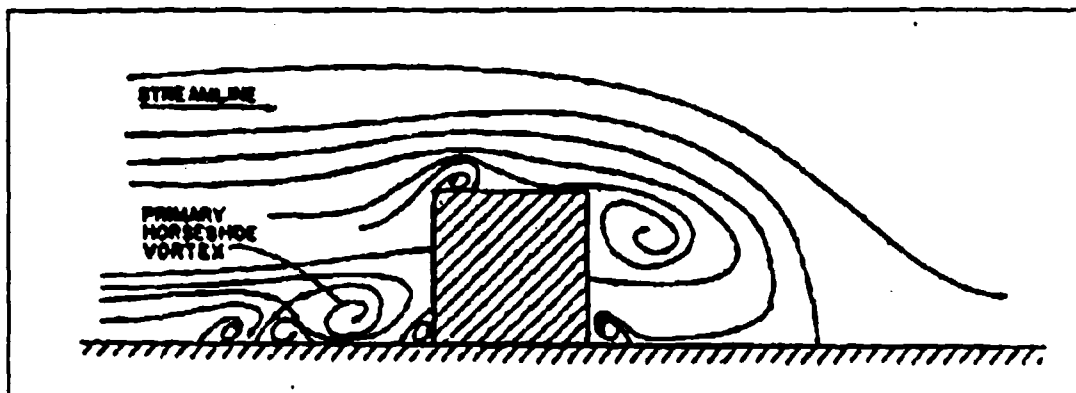


Figure 7. Centerline Streamline Patterns for Flow Reattaching to Top [Ref. 10]

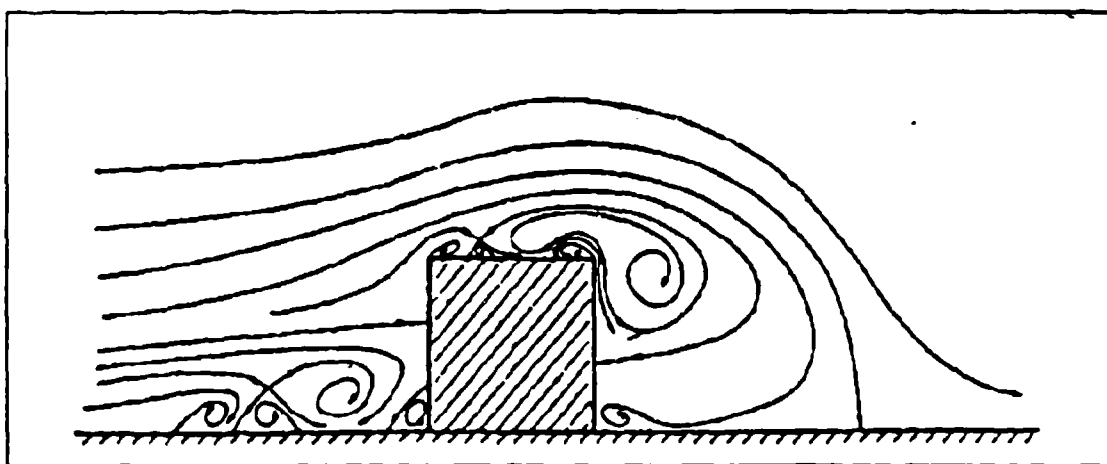


Figure 8. Centerline Streamline Patterns for Flow Not Reattaching to Top [Ref. 10]

object. Near these edges, it separates and may or may not reattach before reaching the back edge. This reattachment depends on many factors such as building-length-to width

ratio, height-to-length ratio and upstream roughness (which also determines the turbulence intensity in the approaching wind). Figures 5 and 7 show flow patterns for attached flow and Figure 8 shows flow patterns for unreattached flow.

A separation cavity covers the rear face of the object. The cavity length is defined by the distance from the building to the centerline reattachment point downwind of the body, and is normalized by the building height. It can vary from two to six building heights [Ref. 8]. As a result of this variation, the reattachment "point" is more accurately called a reattachment zone. This subject will be looked at more closely later.

Obtaining a clear picture of this separation cavity is quite difficult due to the high level of turbulence inside this region. Figure 9, which graphically depicts the streak lines of helium bubbles, is a photograph of a helicopter deck from a flow-visualization study of a DD-963 class destroyer model. Bearing in mind that the size of the cavity changes with ship yaw angle and, to some degree, with pitching and rolling of the ship, it is little wonder that creating an accurate rotor engage/disengage envelope has been both difficult and unsuccessful.

#### C. FLOW OVER A BACKWARD FACING STEP

The next logical step is to proceed and review any studies done on the flow over a backward facing step (BFS). Not only is this type of flow probably the easiest reattaching-flow



Figure 9. Wake of Hangar; DD-963 [Ref. 7:p. 73]

scenario to observe but, it also comes very close to resembling the flow over the centerline of the helicopter deck on the back of the AOR. Luckily, there have been several different type studies of this BFS and it has been established as a "benchmark problem" for checking CFD codes. However, the present review will be confined to those which were restricted to turbulent two-dimensional freestream flow.

Although the backward facing step is the simplest of the reattaching flows, that fact is in no way indicative of the complexity of the flowfield; it is still a very complex flow, as is illustrated by Figure 10. It can be observed that the upstream boundary layer separates at the sharp corner forming

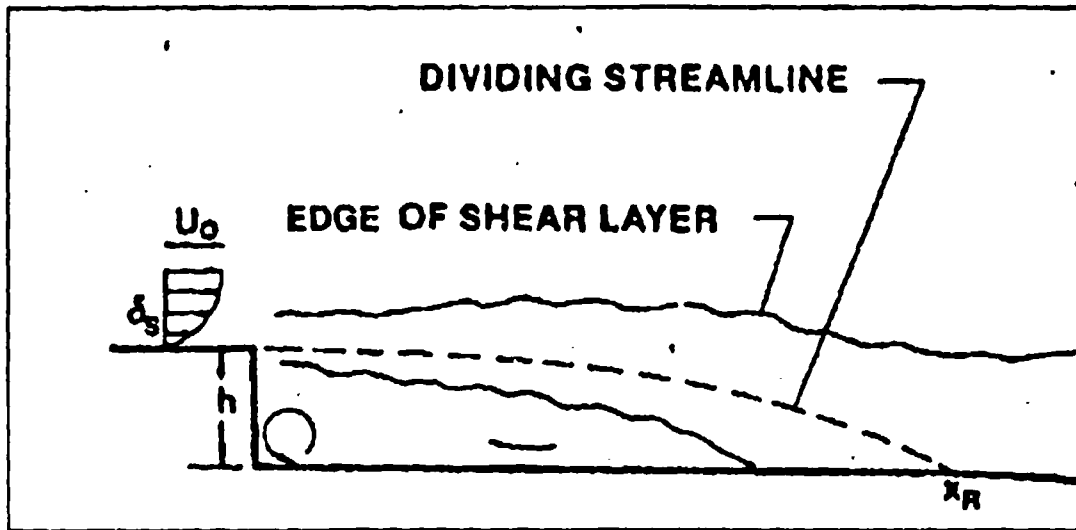


Figure 10. Backward Facing Step Flowfield [Ref. 13]

a shear layer [Ref. 13]. This separated shear layer curves sharply downward in the reattachment zone. Then after striking the floor, part of the flow is deflected upstream into the recirculating flow by a strong adverse pressure gradient. It would be incorrect to consider this recirculation area as a dead air zone. Backward flow has been measured at over 20% of the mean freestream velocity. [Ref. 13]

Eaton and Johnston [Ref. 13] have compared the results of several studies [Refs. 14-16] concerning the reattachment length, which together with the level of turbulence inside the recirculation area, are probably the most important parameters that characterize this flowfield. This work gives insight

into the effect of varying the following four independent parameters: initial boundary-layer state, initial boundary-layer thickness, freestream turbulence and the aspect ratio.

It was found that the effect of changing the state (laminar/turbulent) of the separation boundary layer had a significant effect on the reattachment length (see Figure 11). The flow apparently becomes independent of Reynolds number, based on momentum thickness, when the boundary layer is fully turbulent.

Data, in Eaton and Johnston's study, show that the reattachment length has a weak dependence on the effect of changing the state (laminar/turbulent) of the separation boundary layer. However, four other data sets with different values of the boundary layer thickness, but similar other parameters, show the reattachment length having a much stronger dependence on the thickness. The data suggest that further study is needed to resolve this issue.

The effect of freestream turbulence on the reattachment length has never been studied systematically. The few data sets that resulted from these studies, and documented in Eaton and Johnston's study, showed that fairly high levels of turbulence seemed to decrease the reattachment length. Again, further investigation is required.

The effect on the reattachment length, of the aspect ratio of the flow apparatus (channel height to step height), was also documented. These studies found that the effect was

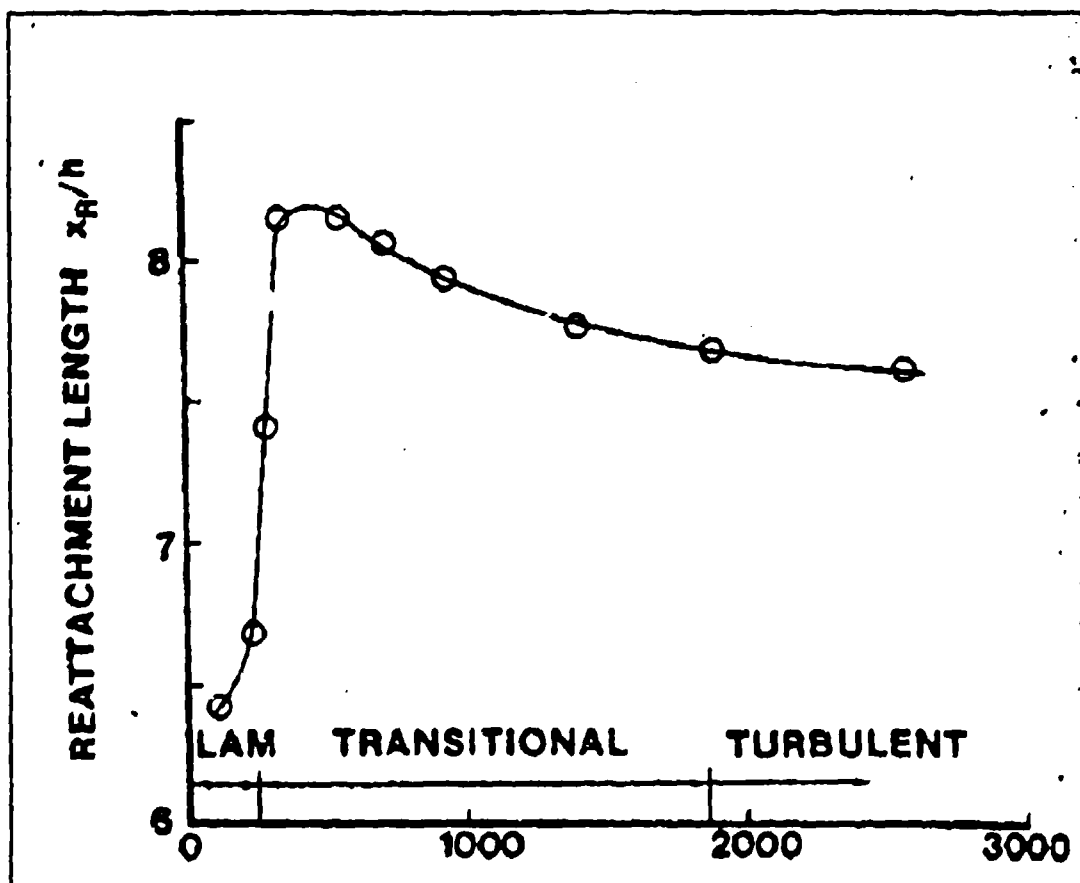


Figure 11. Reattachment-length Measurements Showing Dependence on the State of the Separating Boundary Layer [Ref. 13]

negligible for aspect ratios greater than ten. For aspect ratios less than ten, the reattachment length increases if the boundary layer at separation is laminar and decreases if it is turbulent.

The other important parameter, turbulence in the recirculation area, has also been measured for most of the data sets in Eaton and Johnston's survey. Though there seems

to be a substantial variation in the peak values of turbulence and shear stress, the turbulence-intensity measurements show a consistent pattern when the maximum intensity is plotted as a function of streamwise distance. In almost all cases, the turbulence intensity reaches its greatest value approximately one step height upstream of reattachment and then decays rapidly in the downstream direction.

#### D. FLOW OVER A TWO-DIMENSIONAL OBSTACLE

Since a deflector will be used to direct the airflow over the backward facing step, it would be prudent to spend a brief time looking at the flow over a two-dimensional fence immersed in a turbulent layer on a flat surface. Such a study has been conducted recently by Atli [Ref. 17] who analyzed the flow field through the surface oil technique of flow visualization. He then obtained the longitudinal components of the mean velocities by using hot wire anemometry and applied corrections for flow reversal and turbulence.

Figure 12 shows the structure described by the flow visualization tests. Primary and secondary recirculation regions exist, both upstream and downstream of the fence, with the downstream one considerably larger. He observed that the relative height of the obstacle, in terms of the reference boundary layer and consequently the Reynolds number based on the height of the obstacle, are the parameters affecting the shape of the flowfield and the structure of the turbulence.

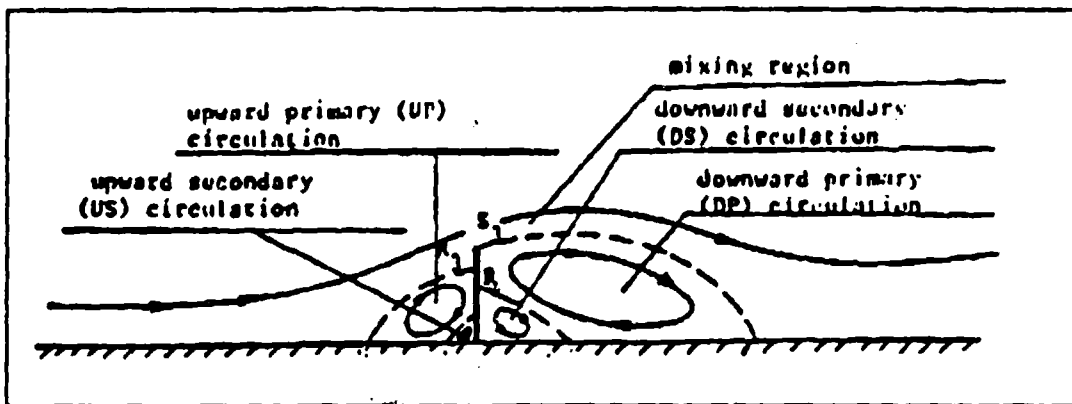


Figure 12. Flow Structure Over a 2-d Fence [Ref. 17]

Specifically the data indicated that the relative length of the primary recirculation region slightly increases when the relative height of the obstacle, and consequently the Reynolds number based on obstacle height, increases. He did not observe this effect for the other recirculation areas; in fact, they remained the same size for the changes made.

Atli went on to compare his work with that of Sinha et al. [Ref. 18] who worked with flow over a backward facing step. He discovered that for 2-d flows with the same value of Reynolds number, the length of the primary recirculation region downstream of a fence on a flat surface is longer than that on the backward facing step. The reason for this is the flow approaching the obstacle diverges from the horizontal before reaching the obstacle because of the upstream



recirculation region. The flow approaching the backward facing step is horizontal and does not diverge.

Another conclusion which Atli reaches, which has some relevance to the present study, is that the reverse velocity profile in the recirculation region increases with height of the step and therefore with the height-based Reynolds number. This increase in obstacle height and Reynolds number also increases the maximum turbulence intensity in the mixing region.

#### E. FLOW MODIFICATION

Though no studies can be found that attempt to modify the airflow over a backward facing step through the use of deflectors, there have been several studies of the airflow over and through fences and shelterbelts. These studies generally deal with modifying the airflow, so as to protect crops or provide comfort for humans, through the use of various type windbreaks. Much of this information is applicable to our current study and will be used in the modelling portion of the problem.

Windbreaks and shelterbelts have played, and continue to play, an important part in protecting man and his environment. It was with this in mind that the World Meteorological Organization, at its second session in 1958, first set up a working group on windbreaks. They worked out a plan for long-term experiments to assist in regional planning of windbreaks

and shelterbelts for research purposes. The results of their work were published in 1964 [Ref. 19] and much of what they concluded is still valid today.

One of the general conclusions of their study was that beneath the peak airflow over a windbreak is the zone of greatest wind reduction (see Figure 13). At that time it was called a "dead calm area" by Kreutz. [Ref. 19:p. 72] This term is really a misnomer, as has since been shown. [Ref. 17] Figure 14 illustrates the reduction in horizontal wind behind a windbreak as a function of windbreak permeability. This figure also shows that the lower the porosity of the obstacle, the nearer to the obstacle the "calm" area is located.

The crucial parameter for wind reduction behind shelterbelts was, therefore, determined to be the shelterbelt's density, or porosity. The less porous, the more wind reduction, but for only a very small area immediately behind the shelterbelt. Then, as the porosity increases, the horizontal wind velocity increases slightly, but the area of protection, measured downwind, also increases. The overall best protection, which extended six to seven shelterbelt heights downstream, was thought to be about 50% porosity.

In 1981 Perera [Ref. 20] showed that the normalized mean wind velocity through a porous fence was independent of the form of the fence construction. Small holes, large holes, and even horizontal slat fences seemed to have no significant effect on altering the results for a given porosity. Several

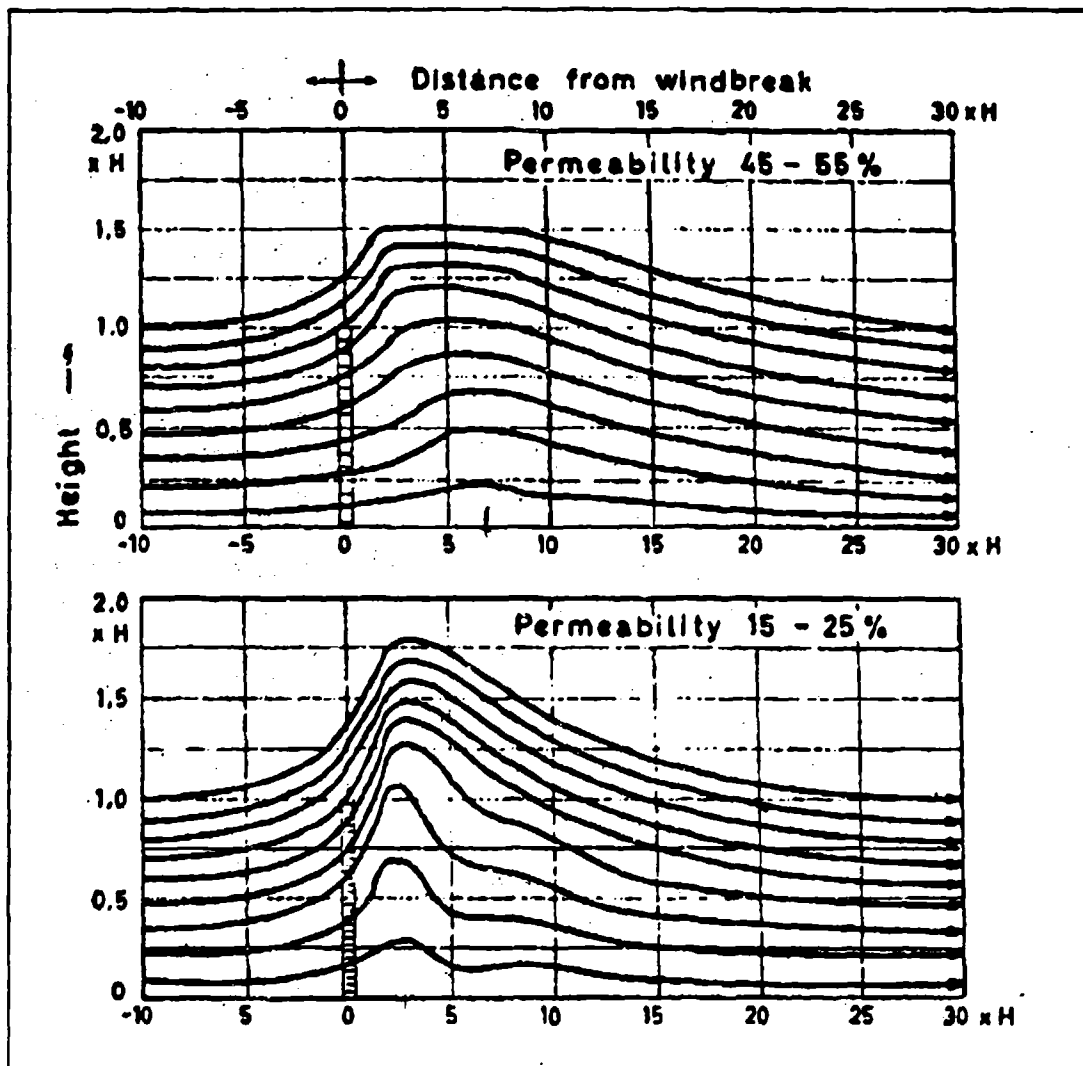


Figure 13. Mean Streamlines at a Medium Dense and a Dense Windbreak [Ref. 19:p. 120]

other studies have also confirmed Perera's results. Another of his conclusions was that, as the porosity increased, the recirculation bubble decreased in size and moved downstream.

His results showed that the recirculation bubble existed only for fences with porosities less than 30%.

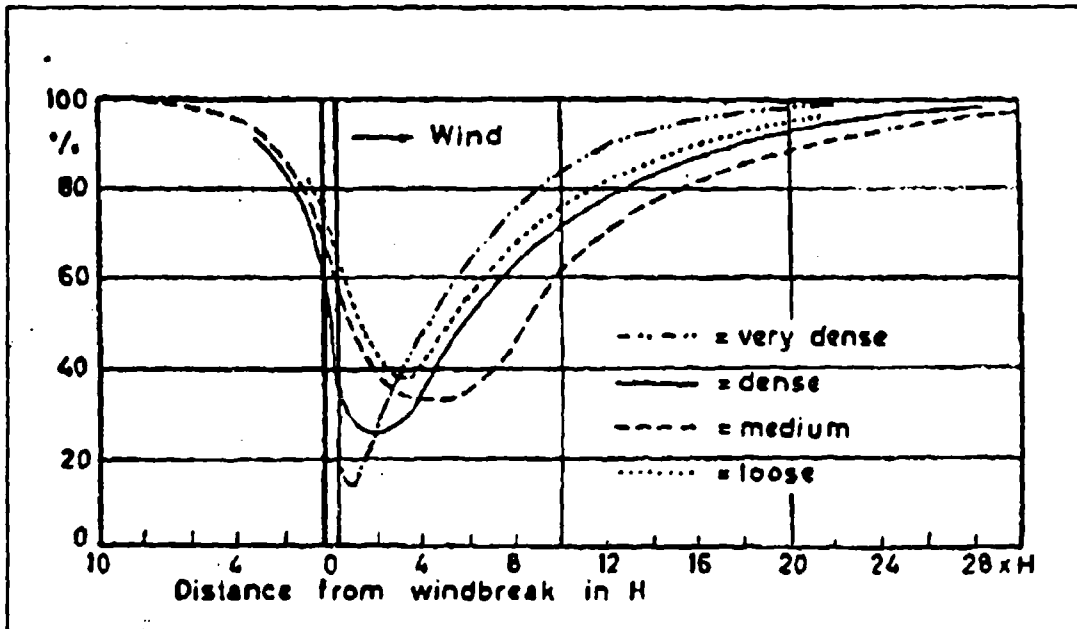


Figure 14. The Wind Speed Reduction of Different Windbreaks ( $H$  = Height of Windbreak) [Ref. 19: p. 120]

To summarize, wake velocities increase with increasing porosity and, in contrast, the turbulence intensity decreases with increasing porosity.

Perera uses a parameter suggested by Gandemer [Ref. 21], which takes into account both the mean and turbulence properties of the wind to determine the best overall porosity for a fence. He (Perera) suggests a fence with a porosity of

about 10%. Interestingly, Gandemer concluded that a fence of 20% porosity provided the best protection, but that a fence of 50% porosity was almost as effective and less expensive to build. It is hoped that all of these porosity parameters can be compared during the computer-modeling process.

### III. CFD PROGRAM SETUP

#### A. BACKGROUND

The computational Fluid Dynamics code used for the modelling process was the PHOENICS Flow-simulation code. This code was first created in 1979-80 and released in 1981. [Ref. 22:p. 1.1] It is a computer code which simulates fluid flow, heat transfer, chemical reactions and related phenomena. The latest version of PHOENICS, 1.5, dated September 1989 was utilized as well as PHOENICS "Easy Flow," a problem definition and management program. Easy Flow uses a menu-driven, graphical interface for problem setup, which is interfaced with the PHOENICS code. This greatly simplified setting up the problems by eliminating the tedious and long task of writing new code each time a minor change was made to the problem.

PHOENICS consists of two essential computer codes and four auxiliary ones. The essential codes consist of a pre-processor called SATELLITE and a processor called EARTH. The auxiliary codes are post-processors called PHOTON, AUTO PLOT and PINTO, and a separate self-instruction program called GUIDE. [Ref. 22:p. 2.3]

SATELLITE is an interpreter; from instructions provided by the user it creates a data file, Q1 (see Appendix), containing instructions which EARTH can obey.

EARTH contains the main flow-simulating software. It incorporates coding sequences which represent the relevant laws of physics applied to elements of material distributed in space and time [Ref. 22:p. 2.3]. EARTH reads the Q1 file provided by SATELLITE and executes the corresponding calculations. It then produces an output file called RESULT, which the user can read or have sent to another file called PHIDA.

The PHOTON code is an interactive program which picks up the PHIDA file written by EARTH and then, in response to instructions entered by the user through the VDU keyboard, represents the computed grid and flow pattern graphically on the screen.

#### B. HOW "PHOENICS" WORKS

PHOENICS describes phenomena involving the flow of heat or material in terms of distributions in space and time of temperatures, velocities, pressures, and other physical quantities. These are the dependent variables. These distributions involve ascribing numerical values to the variables at each of an orderly array of locations, called "nodes" or "grid points." [Ref. 22:p. 2.4]

The printed or plotted values of temperatures, velocities, etc., produced by PHOENICS represent solutions of a set of algebraic equations representing the relevant laws of physics for the chosen set of cells (grid points) (see Figure 15).

These laws are those governing the conservation of mass, momentum and energy, coupled with the transport laws describing heat conduction, diffusion of matter, and viscous action [Ref. 22:p. 2.4].

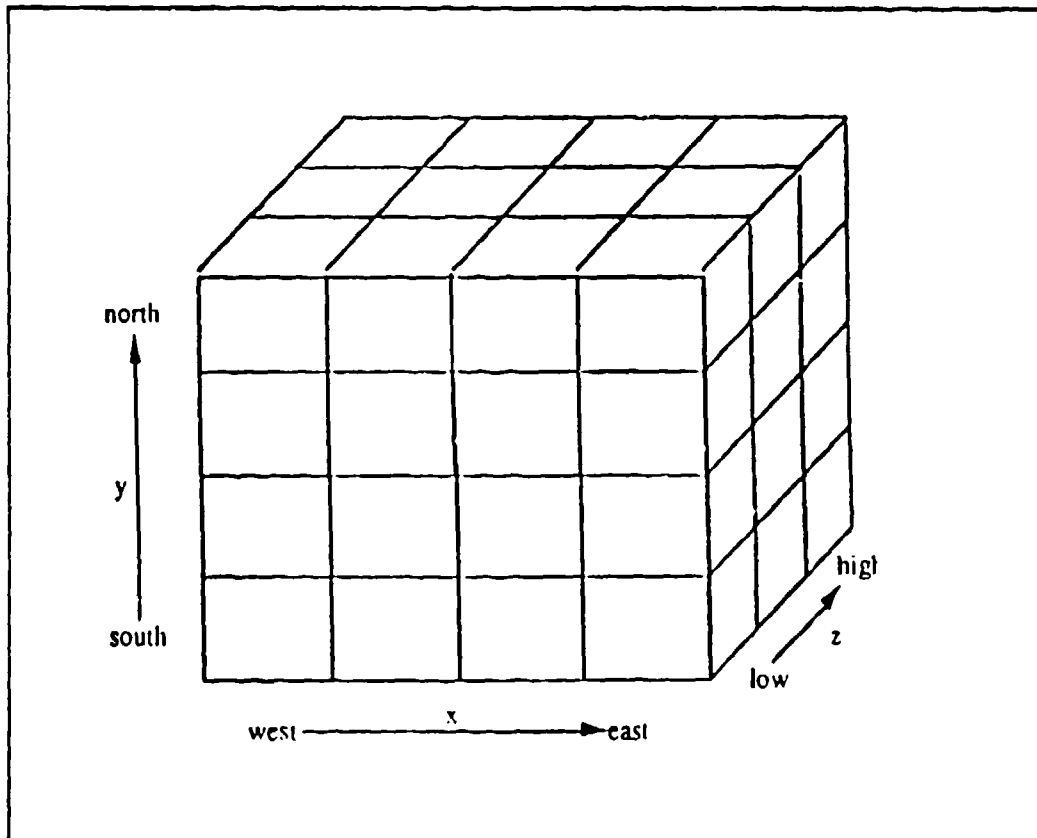


Figure 15. Cell Depiction [Ref. 22:p. 1.11]

In the present study, no conduction nor diffusion nor reactions are considered and the relevant equations are the incompressible, constant viscosity time averaged Navier-Stokes



equations; discretized via a control volume formulation into the generic form:

$$\phi_P = \frac{a_E \phi_E + a_W \phi_W + a_N \phi_N + a_S \phi_S + a_H \phi_H + a_L \phi_L + a_T \phi_T + S}{a_E + a_W + a_N + a_S + a_H + a_L + a_T + a_P} ,$$

where  $\phi$  represents the dependent variable currently in question. The subscripts P, E, W, N, H, and L denote the location at which this variable is computed, in accordance with the north-south-east-west-high-low convention used in PHOENICS [Ref. 22:p. 2.2].

For each dependent variable there are as many algebraic equations as there are cells in the discretized grid domain. For example, in a typical two-dimensional problem with 100 cells in both the X and Y directions, and five dependent variables (from conservation equations), there would be 50,000 algebraic equations to be solved. In addition to being numerous, these sets of equations are strongly coupled through convective terms. PHOENICS solves the discretized equations through an iterative method reducing the imbalance between the right and left sides of every equation to a magnitude which is small enough to be considered negligible (i.e., a converged solution). [Ref. 22:p. 2.13]

The iterative process itself is very complex, involving a multi-stage sequence of adjustments of values, repeated many

times. For the problem in this study a "slabwise" solution was directed. "Slabs" are arrays of cells having the same value of the low-to-high coordinate Z. A "sweep" is a set of slab-wise operations conducted in sequence from the lowest slab to the highest. Because the equations for values at one slab ordinarily make reference to values at the next higher slab, later adjustments made at the higher slab will invalidate, to some extent, the adjustments which have just been made at the lower one [Ref. 22:p. 2.11]. It becomes obvious then, that to get a reasonable and accurate solution, many sweeps must be made until, ideally, all equations are in a "perfect balance" (i.e., a converged solution) that further adjustments are unnecessary.

#### C. PROBLEM CONFIGURATION

The goal of this paper is to recommend possible configurations to be used in the next phase of the program, which is an experimental verification of the present results, using flow visualization and measurement techniques, in the NPS low speed wind tunnel. To that end, the problem dimensions used in PHOENICS were tailored as closely as possible to the equipment and physical dimensions available in the wind tunnel.

The backward facing step has a height of 125mm and the deflectors ranged in length from 25 to 50mm. All of these dimensions were incorporated into the PHOENICS program. The

freestream velocity and turbulence profiles were measured in the wind tunnel. These velocity and turbulence profiles are given in Table 1 and represent approximately a 20 m/sec wind over a fully developed sea.

TABLE 1  
FLOW SIMULATION INPUTS

height (m)	velocity (m/sec)	turbulent intensity (%)
0.050	1.91	11.85
0.075	1.92	12.32
0.100	2.05	11.33
0.200	2.36	4.79
0.300	2.40	3.92
0.400	2.47	3.66
0.475	2.56	3.24
0.625	2.62	3.18
0.750	2.72	2.19

Freestream\* kinetic energy =  $k_0 = 2.58 \text{ m}^2/\text{s}^2$

Freestream\* velocity =  $u_0 = 2.77 \text{ m/sec}$

Freestream\* dissipation rate =  $\epsilon_0 = .172 \text{ m}^3/\text{sec}^3$

Boundary layer =  $\delta = .762 \text{ m}$

\* value at top of boundary layer

The turbulence model selected is the k- $\epsilon$  two equation one. This model has been used extensively and the results of Murakami and Mochida [Ref. 24] show that it yields a reasonable representation of the velocity field around a cubic

model. A problem with the  $k-\epsilon$  model was revealed by an experiment conducted by Yeung and Scott. [Ref. 25:p. 27] In that study, the reattachment lengths obtained were under-predicted when compared to actual case studies. They believe this to be an inherent weakness of the two equation model.

The turbulence viscosity is determined from the values of the turbulent kinetic energy  $k$  and its dissipation rate  $\epsilon$  according to:

$$\mu_t = \rho C_\mu \frac{k^2}{\epsilon}$$

where  $\rho$  is the fluid density and  $C_\mu$  is a constant.

The values of  $k$  and  $\epsilon$  are determined from their own transport equations:

$$\frac{\partial}{\partial x_j} (\rho \mu_j k) = \frac{\partial}{\partial x_j} \left[ \frac{\mu_{eff}}{\sigma_k} \frac{\partial k}{\partial x_j} \right] + G - \rho \epsilon$$

$$\begin{aligned} \frac{\partial}{\partial x_j} (\rho \mu_j \epsilon) &= \frac{\partial}{\partial x_j} \left[ \frac{\mu_{eff}}{\sigma_\epsilon} \frac{\partial \epsilon}{\partial x_j} \right] \\ &+ (C_1 G - C_2 \rho \epsilon) \frac{\epsilon}{k} \end{aligned}$$

$$G = \mu_\epsilon \frac{\partial \mu_j}{\partial x_j} \left( \frac{\partial \mu_j}{\partial x_j} + \frac{\partial \mu_j}{\partial x_i} \right)$$

The values of  $C_\mu$ ,  $C_1$ ,  $C_2$ , and the other parameters are given in the nomenclature list.

To establish a baseline on how the results of PHOENICS compare to other 2-d flow studies, two basic configurations were used. The first was a backward facing step without a deflector, for which the inputs are detailed in Table 1. Next, solid and porous fences were considered, the program run, and the results recorded. The porosity, which is the percentage of the deflector area open to airflow, ranged between 15% and 40%.

Deflectors were then introduced into the study in an attempt to tailor the airflow in such a way as to reduce the velocity gradient and the overall turbulence in the region downstream of the step. The first such deflector was 50mm in length and placed 25mm directly above the step's edge (see Figure 16). This configuration, where configuration refers to size, location and orientation of a deflector, was run at different porosities before a new configuration was established and a set of new runs attempted. All of the runs, including deflector size, position, and porosity are documented in Table 2.

Next, in order to create a slanted deflector, Body Fitted Coordinates (BFC) were utilized. An example of such a configuration is shown in Figure 17. The deflector was set at angles of 30 degrees and 45 degrees (measured from the vertical) at different locations and porosities for several runs (see Table 2).

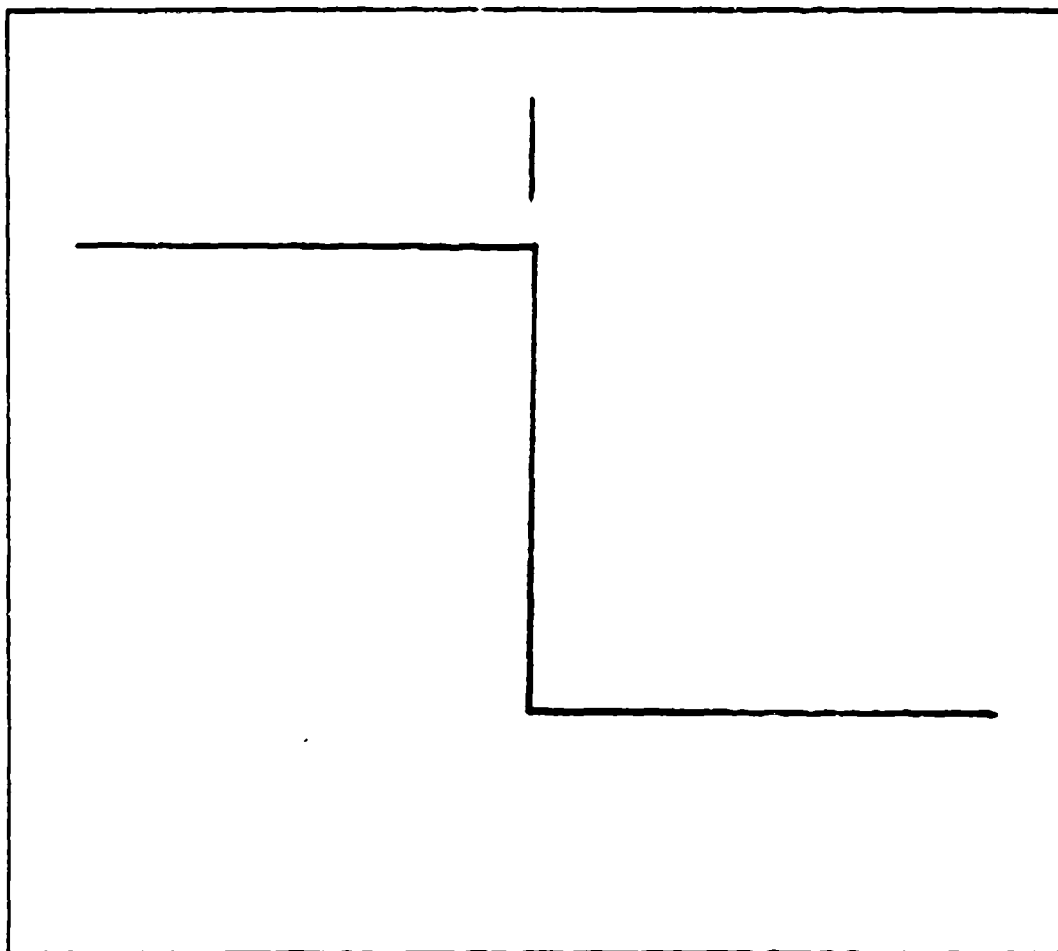


Figure 16. Step with Vertical Deflector

TABLE 2  
DEFLECTOR CONFIGURATIONS

Figure	Deflector/ Fence-length	Porosity (%)	Distance Above-Below Step Edge* (mm)	Offset Dis- tance Down- stream of Step Face* (mm)
18a 18b	-	-	-	-
19a 19b	125	0.0	-	-
20a 20b	125	10.0	-	-
21a 21b	125	20.0	-	-
22a 22b	50	15.0	25.0	0.0
23a 23b	50	0.0	12.5	12.5
24a 24b	50	15.0	12.5	12.5
25a 25b	50	0.0	0.0	12.5
26a 26b	50	5.0	12.5	25.0
27a 27b	25	0.0	0.0	50.0
28a 28b	50	0.0	0.0	50.0
29a 29b	50	5.0	0.0	50.0
30a 30b	50	15.0	-25.0	50.0
31a 31b	50	0.0	0.0	30.0
32a 32b	50	10.0	0.0	30.0
33a 33b	50	0.0	0.0	50.0
34a 34b	50	5.0	0.0	50.0
35a 35b**	50	0.0	0.0	50.0
36a 36b***	50	0.0	0.0	50.0

\* Distance measured from lower edge of deflector

\*\* 30/60 degree cranked deflector

\*\*\* 45/60 degree cranked deflector

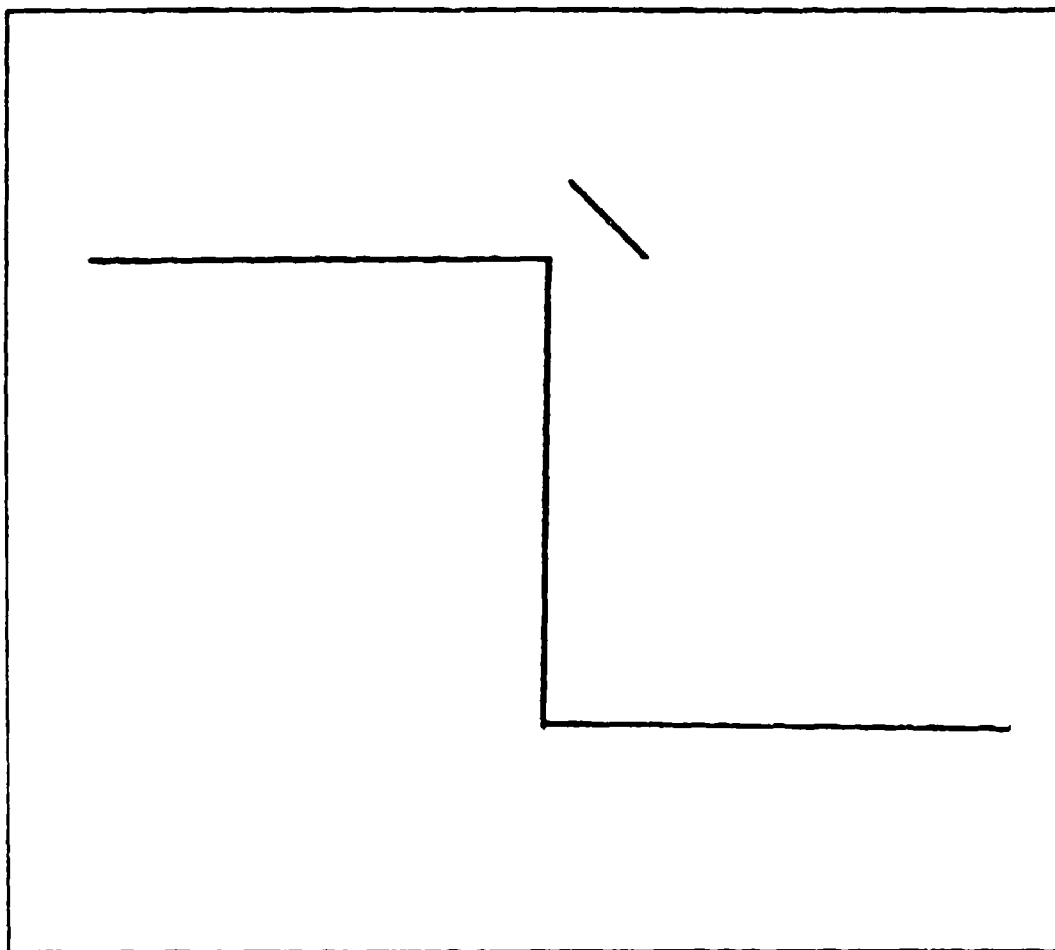


Figure 17. Step with Slanted Deflector



#### IV. RESULTS AND DISCUSSION

The configurations used in the "Phoenix" CFD program are documented in Table 2. Briefly, they were: a backward facing step; a fence set perpendicular to the flow and various deflector arrangements in conjunction with the backward facing step. All runs were allowed to continue the iteration process until such time that the residuals were small enough, or had decreased in magnitude enough, to achieve what was considered balanced equations (converged solution). [Ref. 25 p. 5.26] Residuals refer to the measure of total imbalance of the discretized equations being computed. The number of sweeps to accomplish this varied between 600 and 900.

Initially the code as installed on the COMPAQ DESKPRO 386/25, would complete only a small number of sweeps (between one and 100) before an error statement appeared on the VDU and all iterations ceased. After several weeks of troubleshooting and fruitless calls for assistance to CHAM (the developers of "Phoenix"), it was decided to remove the WEITEK math co-processor which was installed in the computer along with the Intel 80387 math co-processor. CHAM made assurances that the software package sent was specifically designed to be used with both co-processors and that removing the WEITEK co-processor would have no effect. However, when the removal was complete, the "Phoenix" code functioned normally. Other

problems encountered with the "Phoenix" code will be discussed later.

#### A. BACKWARD FACING STEP

The first runs were made simulating airflow over a 125mm high backward facing step (BFS) as shown in Figure 18a and 18b. The velocity vectors and contours of turbulent kinetic energy (TKE) values were plotted for all configurations.

The flow over the BFS closely resembles that which has been documented in the literature previously referenced, with one exception, the reattachment zone. It is located only about 3.5 step heights downstream rather than the four to six step heights achieved in wind tunnel experiments. This is more than likely a result from using the  $k-\epsilon$  turbulence model which, as was stated previously, tends to underestimate the reattachment zone. However, on a positive note, the area of maximum TKE is located approximately one step height upstream from the reattachment zone, as was the case in the literature cited.

These velocity vectors and TKE values of Figure 18 will now be used as a "benchmark" for comparison against all other configurations used. A region of special interest to this study is the region of space that would be occupied by the main rotor blades of the helicopters during start-up and shut-down. Hereafter this region will be referred to as "the region of special interest." It ranges from one-half, to one

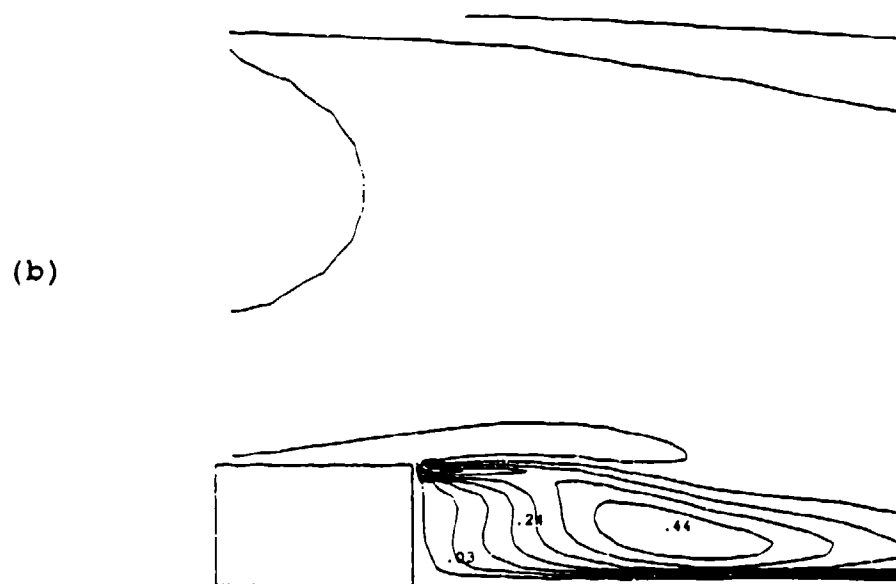
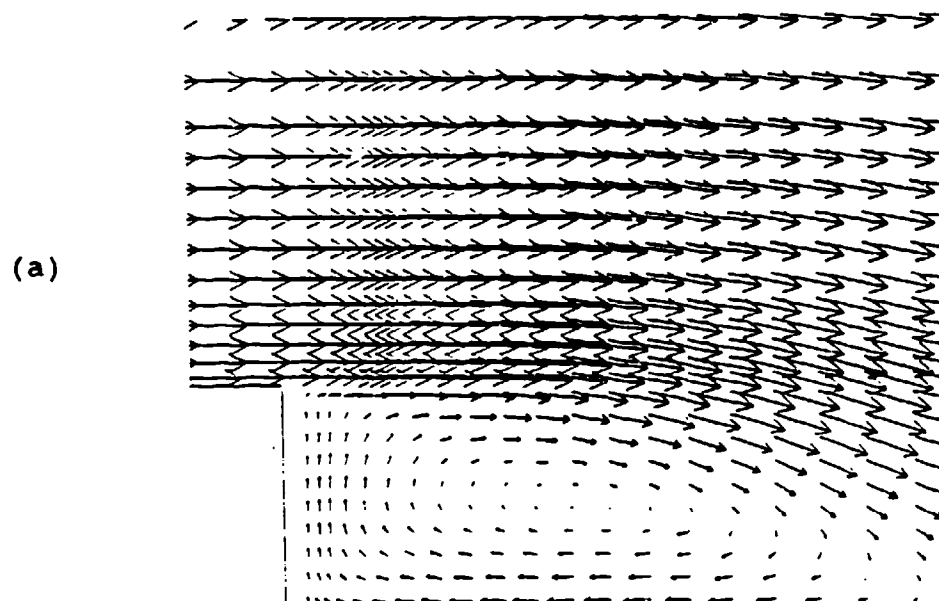


Figure 18. Backward-Facing-Step

full step height downstream of the step and one-fourth, to three-fourths of a step height off the floor. In the discussion that follows, unless otherwise indicated, comparisons of the properties of a given flow and the reference BFS flow refer to this particular area.

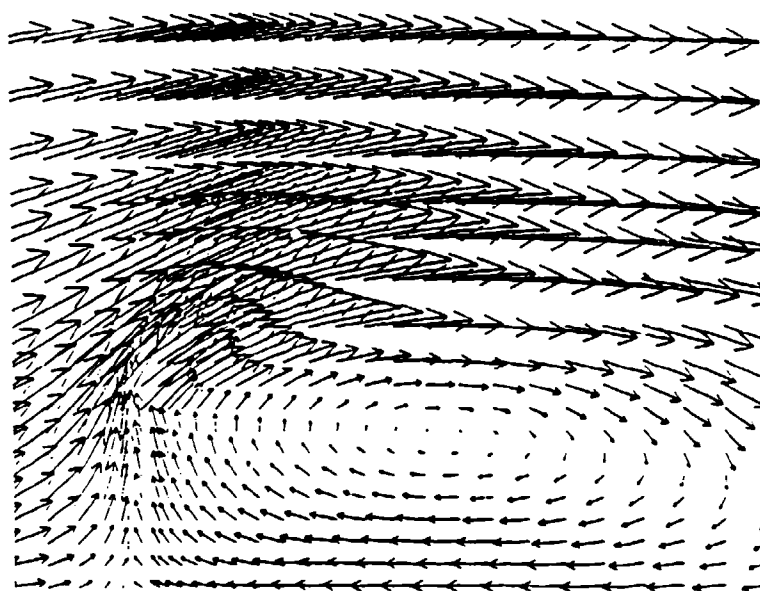
#### B. TWO-DIMENSIONAL FENCE

The flow depicted downstream of the fence has a well-defined recirculation area with reverse flow up to 30% greater than that found downstream of the BFS, and TKE intensities up to 400% greater, as shown in Figure 19a and 19b.

Runs with a 10% porous fence resulted in the primary recirculation area shifting approximately  $1/2$  step heights downstream and a secondary recirculation zone appearing immediately downstream of the fence, as shown in Figure 20a and 20b. Evidence of this secondary zone downstream of a porous fence has not been found in the references cited. The TKE intensities increased greatly in the vicinity of the fence and then quickly dissipated as the flow moved downstream.

As shown by Figure 21a and 21b the 20% porous fence completely eliminated all traces of the recirculation area but the fence had even higher values of TKE around it. Most literature cited had the recirculation area existing until at least 30% porosity was achieved. This discrepancy will have to be further examined when the study moves to the experimental stage.

(a)



(b)

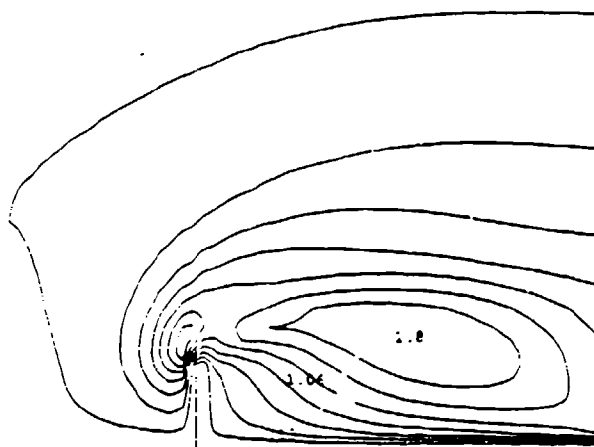
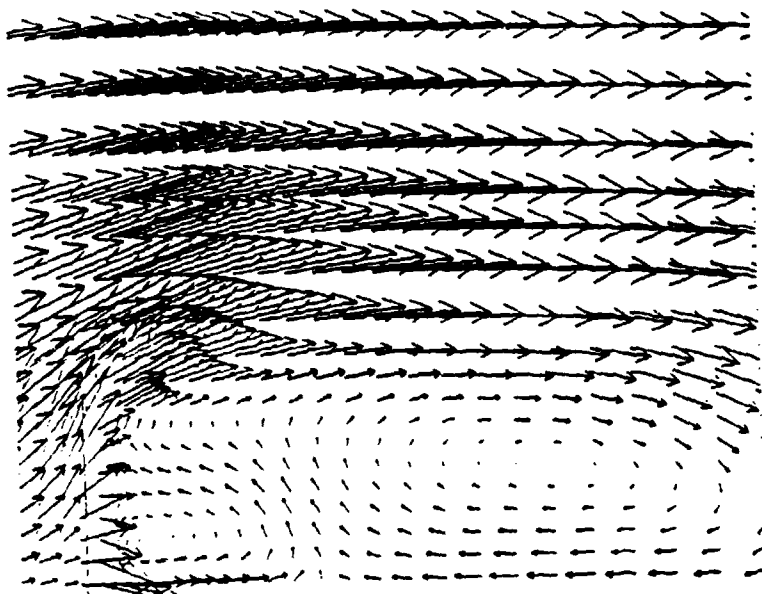


Figure 19. 2-d Fence; 0.0% Porosity

(a)



(b)

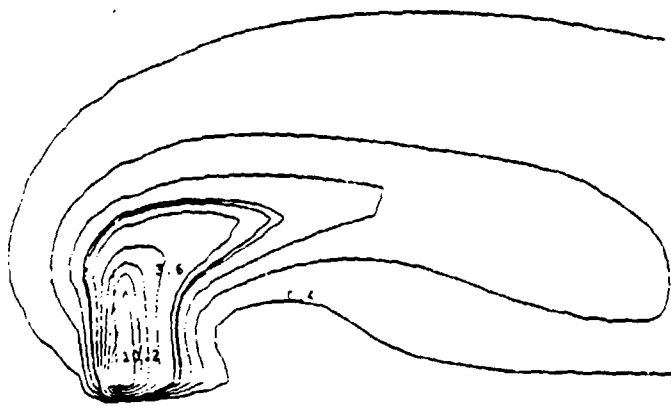
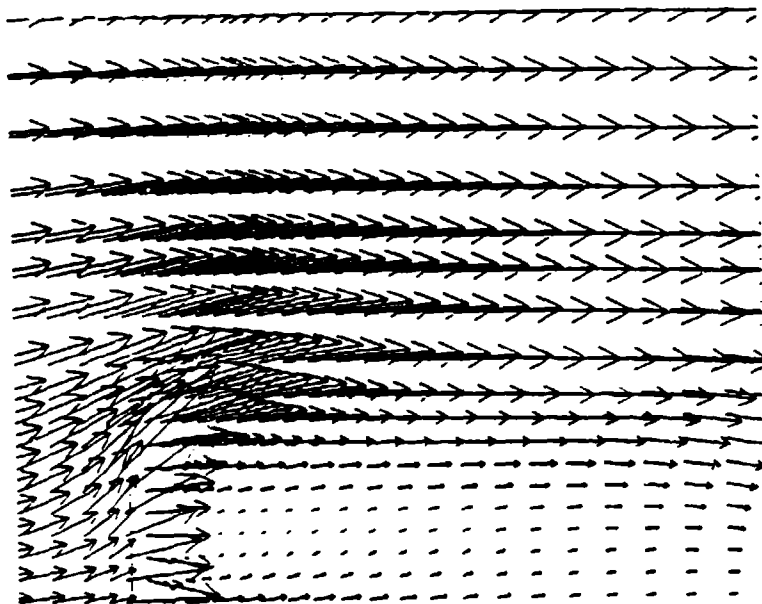


Figure 20. 2-d Fence; 10% Porosity

(a)



(b)

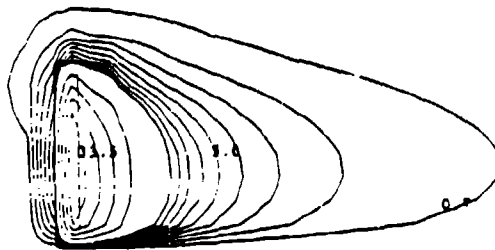


Figure 21. 2-d Fence; 20% Porosity

#### C. VERTICAL DEFLECTOR ABOVE STEP

The first configuration using a vertical deflector was one in which a 50mm deflector was placed 25mm directly above the step. At 0% porosity there was a great deal of recirculation behind the deflector, while at 15% porosity this recirculation was eliminated, as illustrated in Figure 22a and 22b. In both cases, there was little or no effect on the recirculation behind the step. Decreasing the vertical gap (measured from the top edge of the step to the bottom edge of the deflector) to 12.5mm had the same overall results.

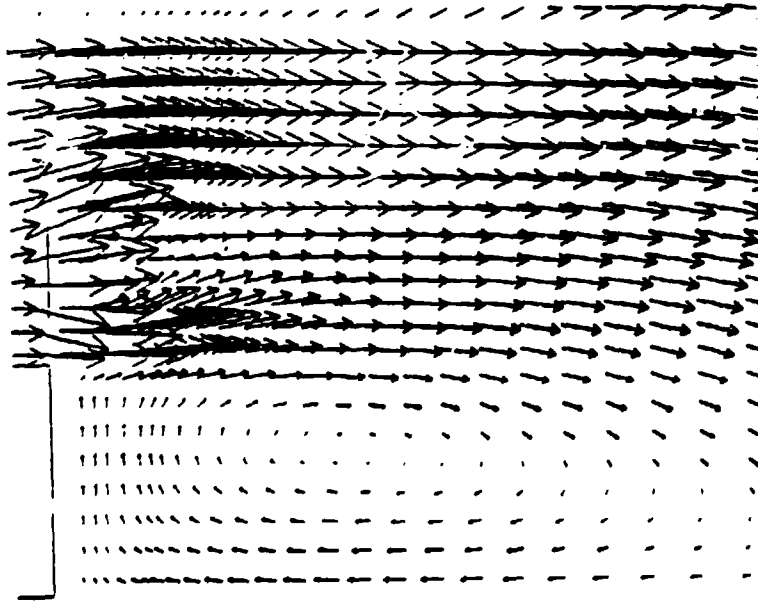
#### D. VERTICAL DEFLECTOR OFFSET 12.5MM

With the vertical gap still at 12.5mm the 50mm deflector was offset downstream of the step by 12.5mm. Figure 23a and 23b indicate that at 0% porosity, a recirculation area exists that is much larger than that found behind the BFS, though it was shifted downstream approximately one additional step height. The velocities in the "region of interest" were, on the average, of the same magnitude as those of the BFS, though the flow vectors were now all moving in the same upward direction. The TKE was very high in the vicinity of the deflector but, near the floor, was lower than for the BFS.

Increasing the porosity to 5%, 10% and then 15% increasingly reduced the recirculation area. At 15% porosity, the primary recirculation area resembles that of the BFS; however, the velocity vectors were all reduced 10%-20% as



(a)



(b)

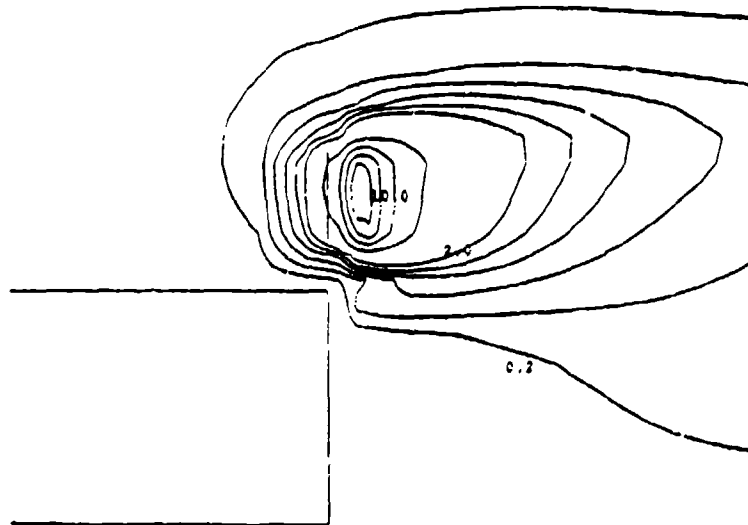
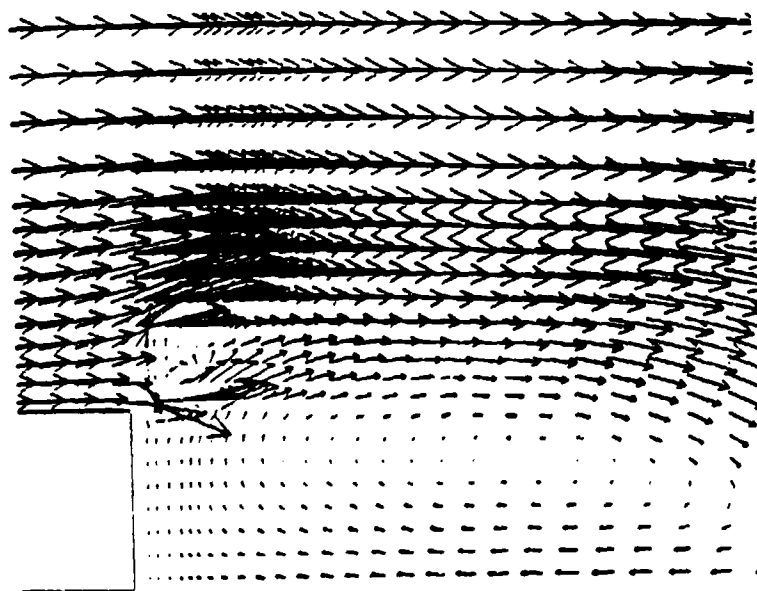


Figure 22. 50mm Vertical Deflector; 15% Porosity;  
25mm Vertical Gap

(a)



(b)

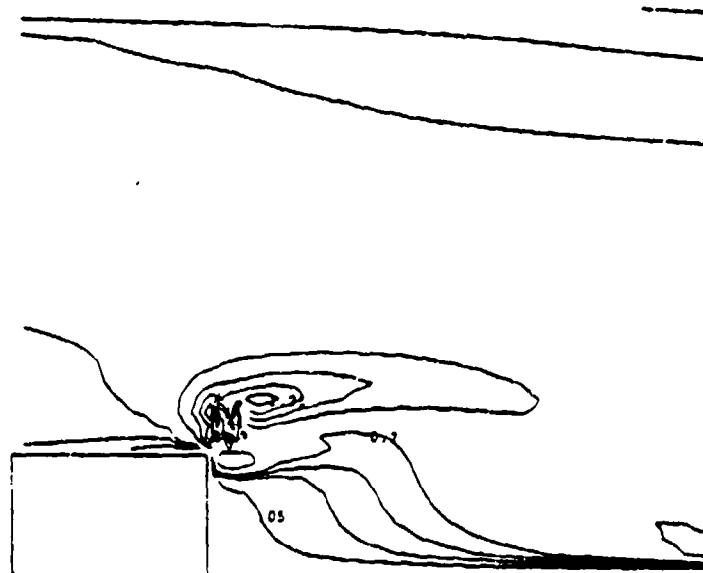


Figure 23. 50mm Vertical Deflector; 0.0% Porosity,  
12.5mm Vertical Gap

shown in Figure 24a and 24b. The TKE was also reduced in "the region of interest."

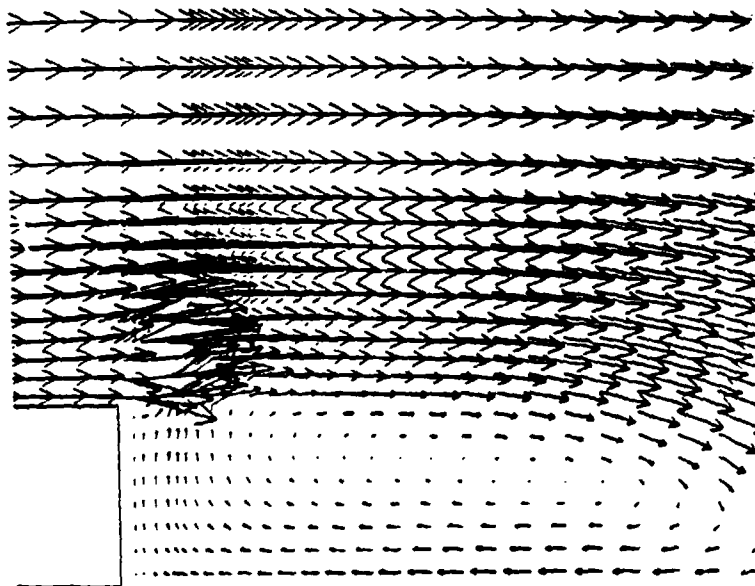
Lowering the deflector so that there was no vertical gap resulted in a very large recirculation area with velocity vectors 20%-30% larger than those found downstream of the BFS (see Figure 25). Interestingly, the TKE intensities remained about the same as the BFS.

It became obvious that, to reduce the primary recirculation zone, the deflector would have to be moved further downstream.

#### E. VERTICAL DEFLECTOR OFFSET 25MM

Moving the 50mm deflector to a position 25mm downstream with a 12.5mm vertical separation and 0% porosity did not give much better results. However, increasing the porosity to 5%, eliminated most of the recirculation downstream of the deflector and reduced the velocity vectors downstream of the step on the average of about 70%, as illustrated in Figure 26a and 26b. This drastically reduced the velocities in the recirculation zone. While the TKE is quite high in the vicinity of the deflector, it dissipates rapidly as the distance increases, and becomes much lower than that of the BFS in "the region of interest."

(a)



(b)

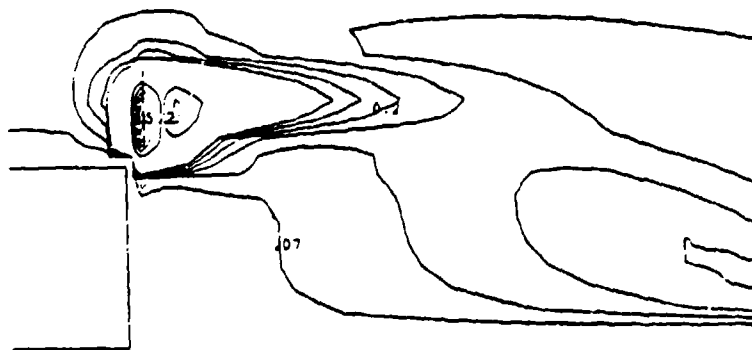
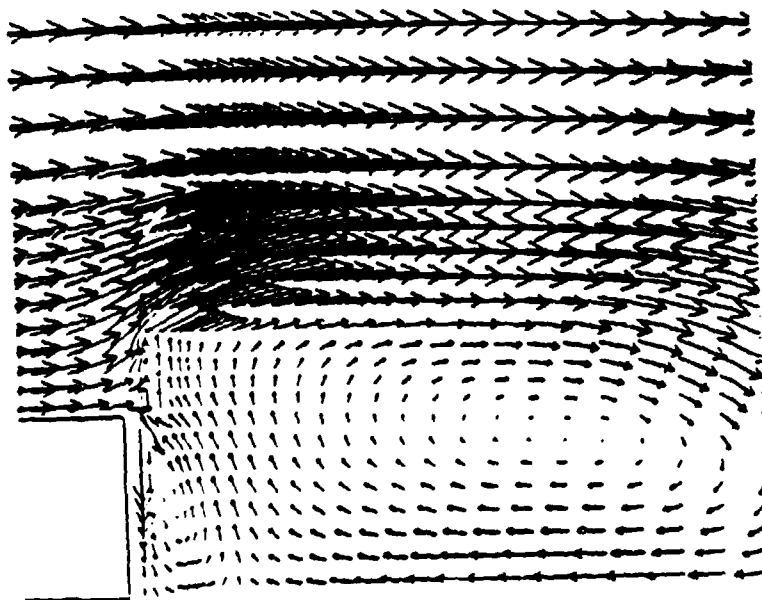


Figure 24. 50mm Vertical Deflector; 15% Porosity, 12.5mm Vertical Gap, 12.5mm Offset Downstream

(a)



(b)

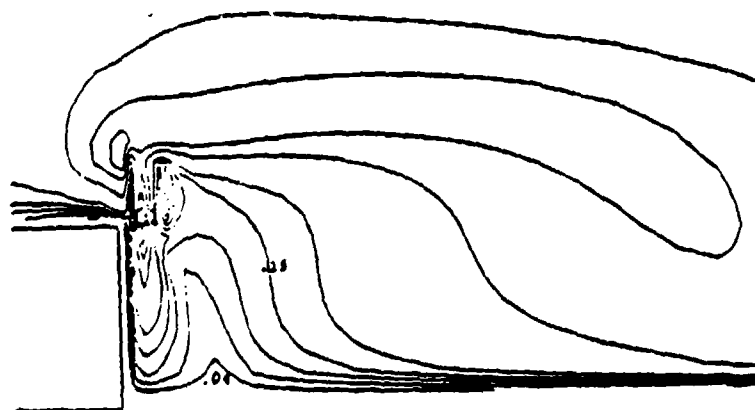
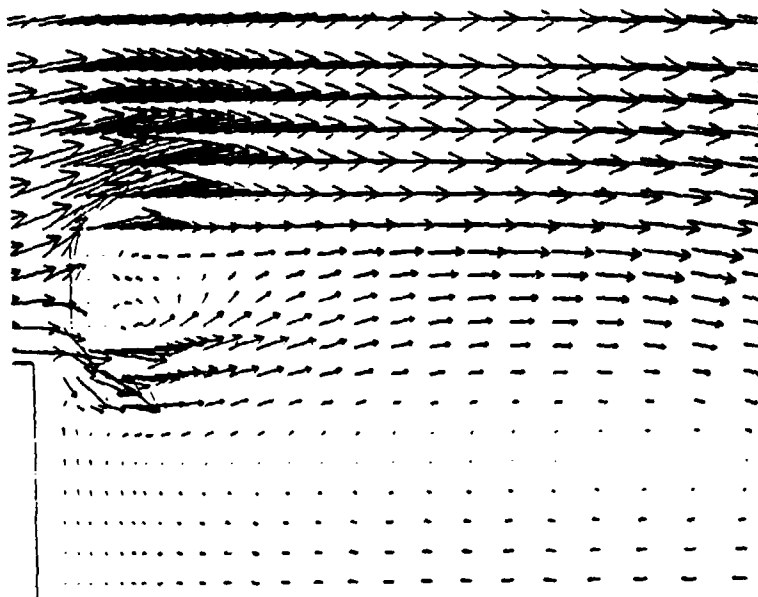


Figure 25. 50mm Vertical Deflector; 0.0% Porosity, 0.0mm Vertical Gap, 12.5mm Offset Downstream

(a)



(b)

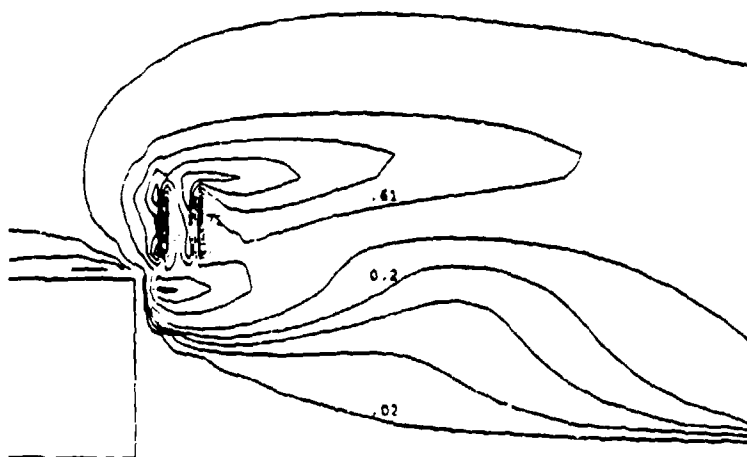


Figure 26. 50mm Vertical Deflector; 5% Porosity, 12.5mm Vertical Gap, 25mm Offset Downstream

#### F. VERTICAL DEFLECTOR OFFSET 50MM

The deflector was moved further downstream to a position 50mm from the step and without any vertical gap. Both 25mm and 50mm deflectors were used with different results.

The 25mm deflector at 0% porosity channeled the airflow in such a way as to eliminate the primary recirculation zone, as seen in Figure 27a and 27b, but a smaller and weaker recirculation zone, with little TKE was formed at the base of the step. In "the region of interest" the flow is predominantly downward with a velocity magnitude such that is found at the downstream end of the BFS recirculation zone. The TKE is approximately the same as that found in the BFS, but was much lower near the floor. Increasing the porosity, even to 5%, increased the airflow enough to reform the large primary recirculation zone.

Increasing the size of the deflector to 50mm and setting the porosity to 0% eliminated the secondary recirculation zone at the base of the step, but another small zone appeared slightly below and downstream of the deflector; this is illustrated by Figure 28a and 28b. The flow is now directed downward with localized velocities under the deflector and with the TKE up to four times that found downstream of the BFS.

By increasing the porosity to 5% the secondary recirculation zone is eliminated, but there still remains a low velocity "S" type flow pattern, as seen in Figure 29a and 29b.

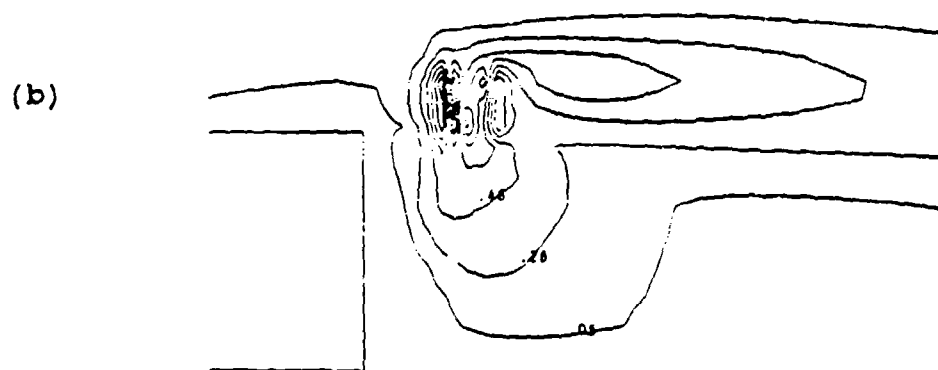
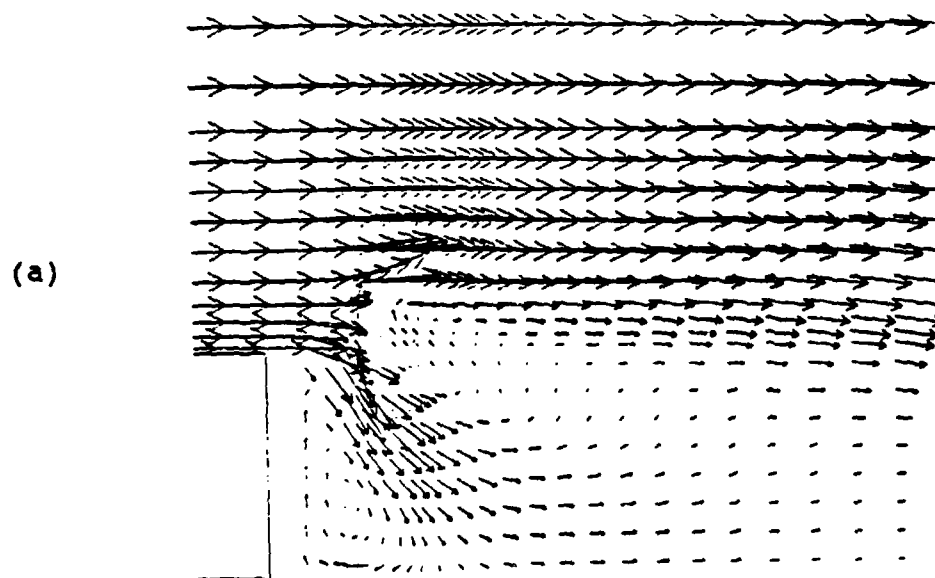


Figure 27. 25mm Vertical Deflector; 0.0% Porosity, 0.0mm Vertical Gap, 50mm Offset Downstream



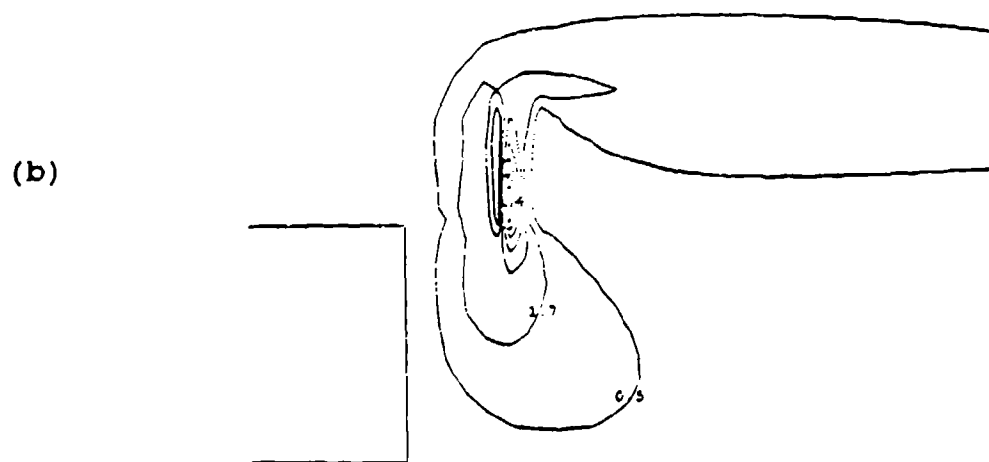
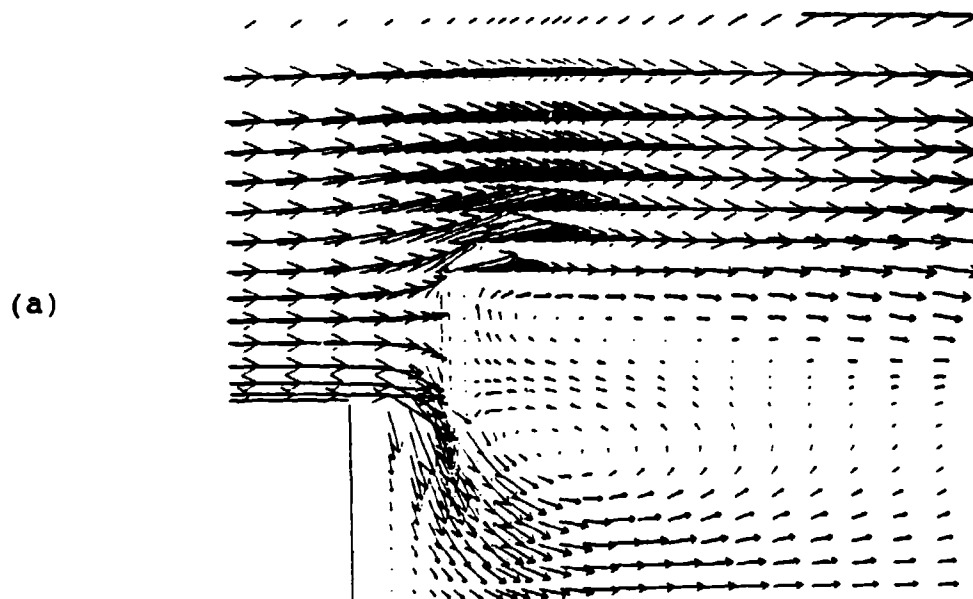
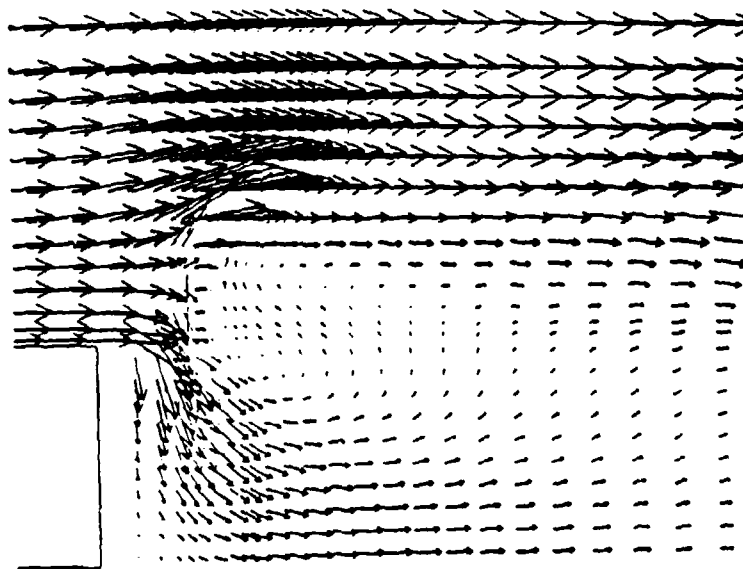


Figure 28. 50mm Vertical Deflector; 0.0% Porosity, 0.0mm Vertical Gap, 50mm Offset Downstream

(a)



(b)

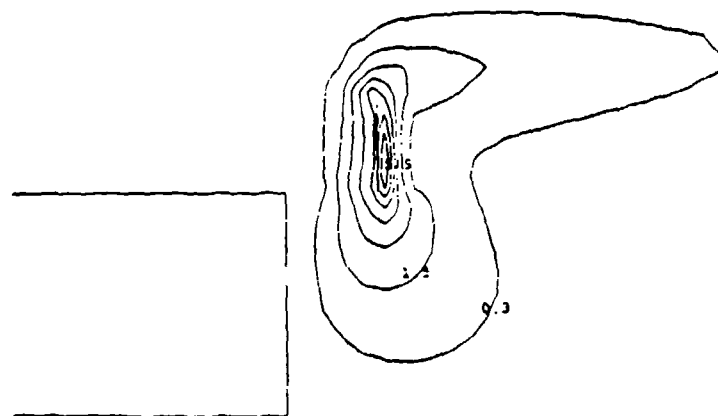


Figure 29. 50mm Vertical Deflector; 5% Porosity, 0.0mm Vertical Gap, 50mm Offset Downstream

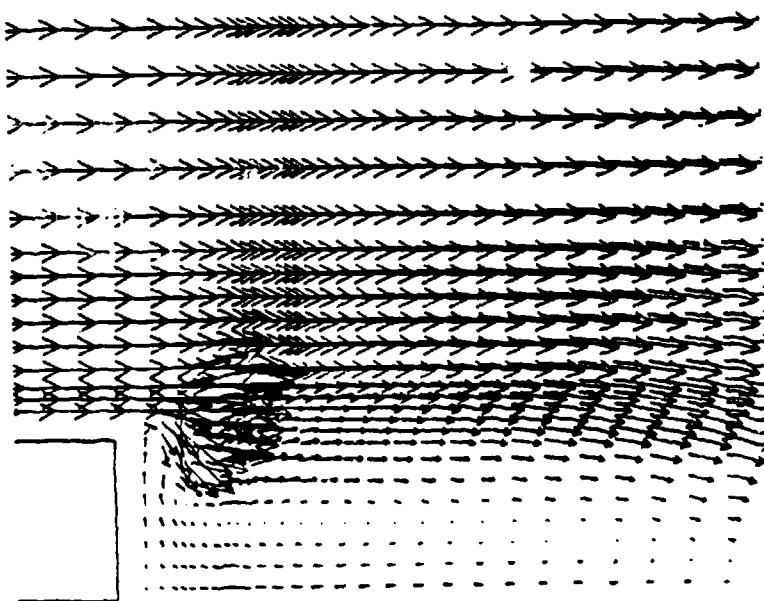
The TKE is slightly lower than the previous example but still far greater than what is found downstream of the BFS. Increasing the porosity any further allows the primary recirculation zone to reappear with both velocity vectors and TKE substantially higher than the BFS.

An additional configuration was considered, in which a 50mm deflector was again offset 50mm, but now placed such that half of the deflector was above the step and 1/2 below. The only run that had an interesting effect was the 15% porous deflector. The primary recirculation zone, as shown in Figure 30a and 30b was almost eliminated, though a small, weak, remnant is still evident further downstream. An "S"-type flow pattern is formed with velocity and TKE magnitudes approximately the same as the BFS. However, the velocity vectors do not start their upward flow until much further downstream.

#### G. SLANTED OFFSET DEFLECTORS

The first such slanted deflector was offset 30mm and angled back 30 degrees (see Figure 31). Remnants of the original primary recirculation zone are just visible at the right edge of the figure. Another "S"-type flow can be observed with velocities of about the same magnitude as those of the BFS; in essence, there are two recirculation zones with opposite sense, one being stronger than the other. The TKE in "the region of interest" is much lower than that of the BFS.

(a)



(b)

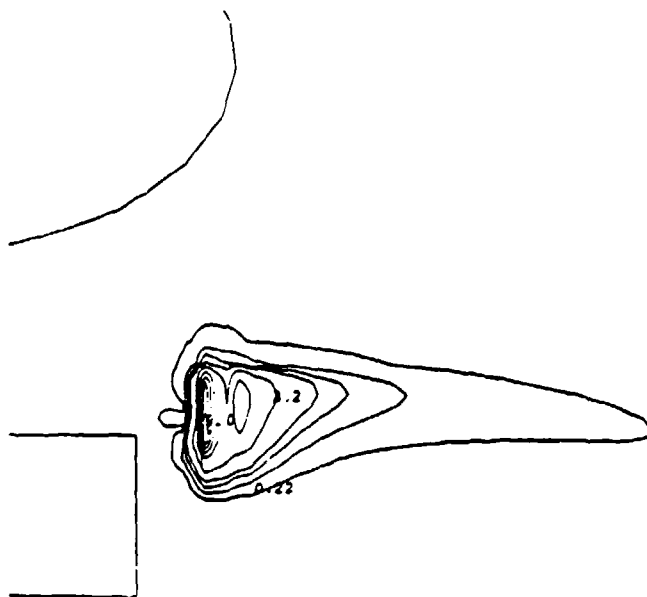
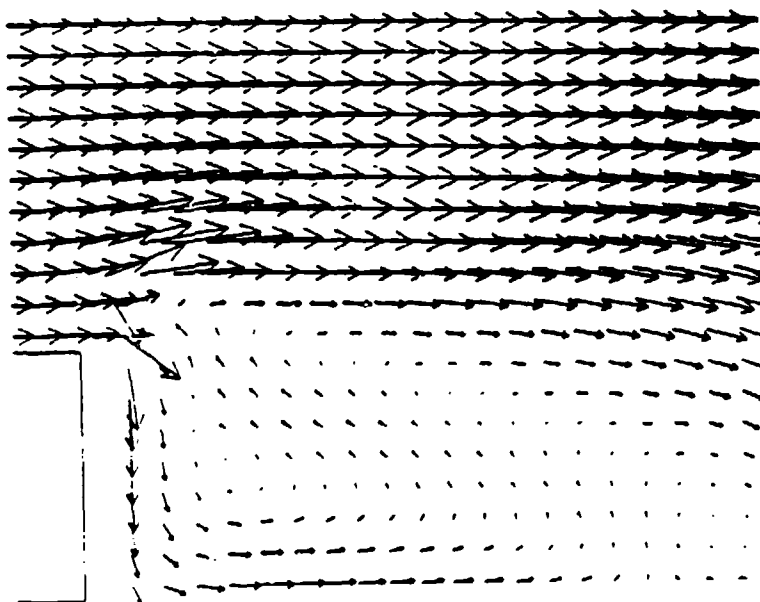


Figure 30. 50mm Vertical Deflector; 15% Porosity,  
Bottom Edge -25mm Below Step Top,  
50mm Offset Downstream

(a)



(b)

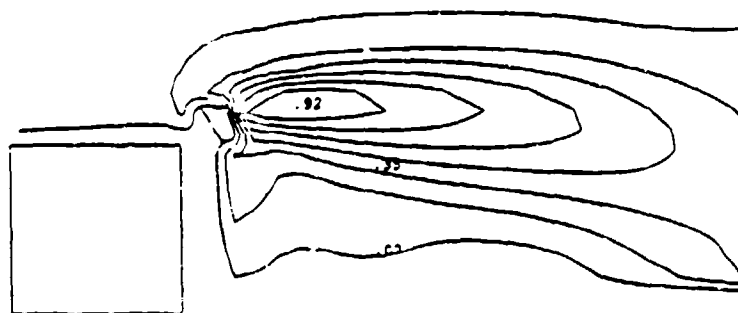


Figure 31. 50mm Deflector Slanted 30 Degrees; 0.0% Porosity, Bottom Edge 30mm Offset Downstream

It is interesting to note that "Phoenix" does not predict any measurable flow immediately along the back of the step while using the angled deflectors. This was not the case when using the straight vertical deflectors.

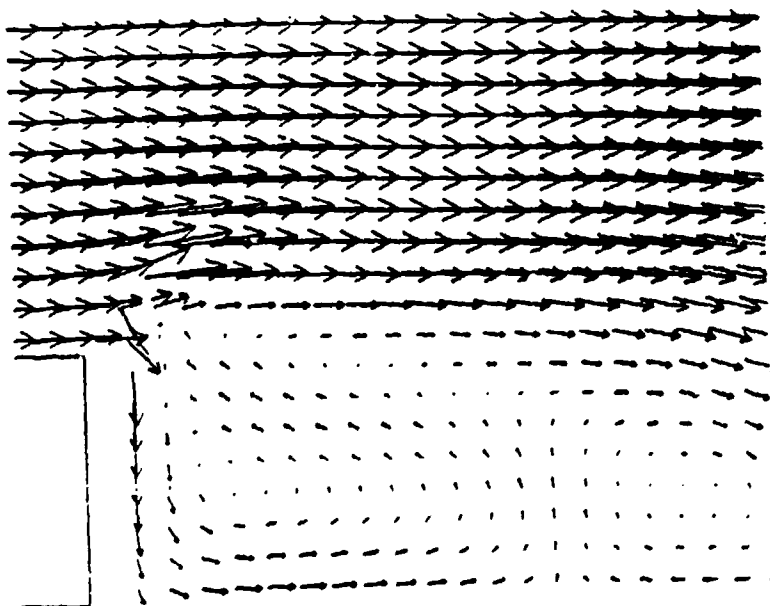
Increasing the porosity to 10% and above, increased the size of the displaced primary recirculation zone so that there are now two significant zones of recirculation to contend with. These are illustrated in Figure 32a and 32b. The TKE, apart from the vicinity of the deflector, is much lower than for the BFS.

The offset distance was increased to 50mm, and at 0% porosity the primary recirculation zone is again shifted downstream as shown in Figure 33a and 33b. It appears to be extremely weak and of little consequence. The "S" pattern is again evident but observing "the area of interest" the flow is fairly uniform with the TKE approximately the same magnitude as the BFS.

On increasing the porosity to 5%, not only has the primary recirculation zone become more pronounced, but the "S" flow velocity vectors have increased on the order of 25%-40% with a corresponding increase in the TKE (see Figure 34). A similar trend occurs at higher porosities.

The final two configurations were cranked-type deflectors. In the first instance the lower part of the deflector is angled at 30 degrees to the vertical and the upper at 60 degrees to the vertical, as shown in Figure 35a and 35b. The second case

(a)



(b)

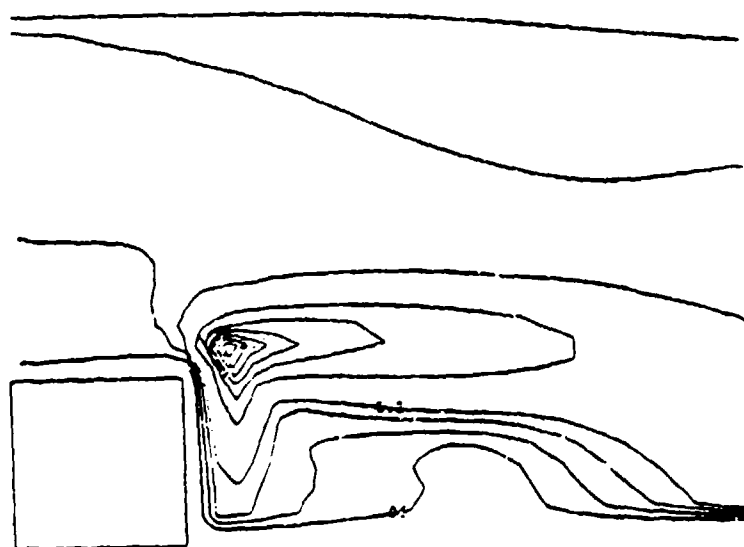
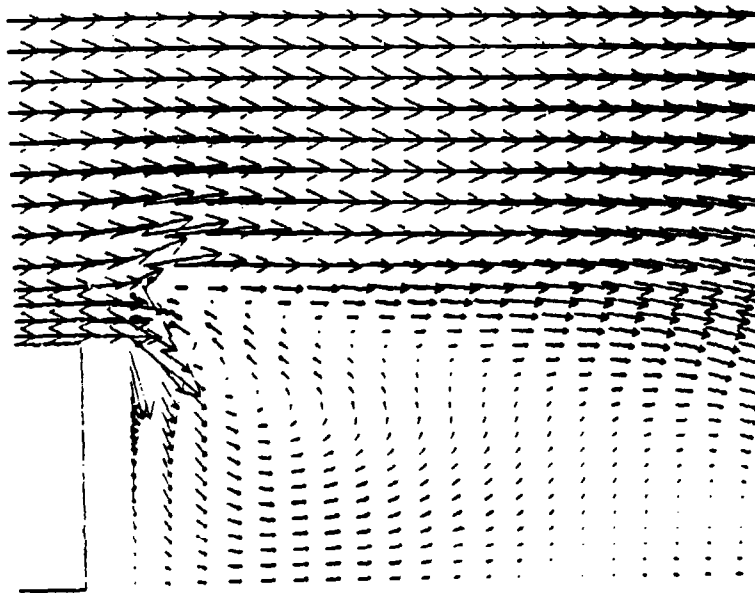


Figure 32 . 50mm Deflector Slanted 30 Degrees; 10% Porosity, Bottom Edge 30mm Offset Downstream

(a)



(b)

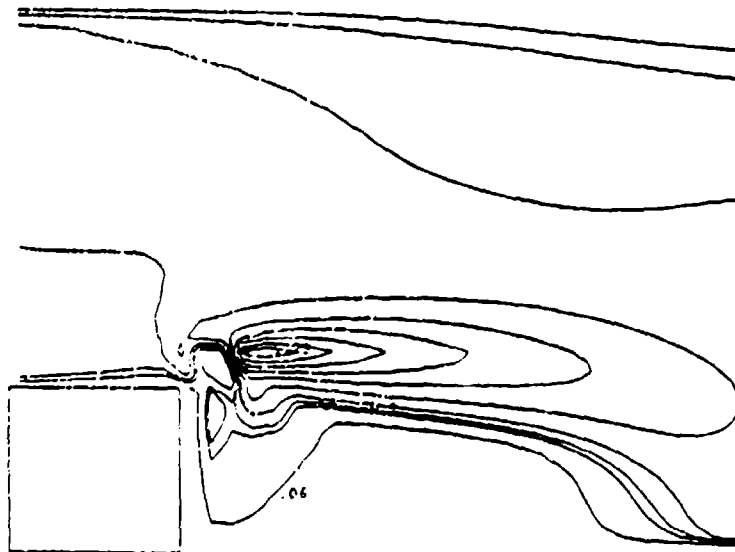
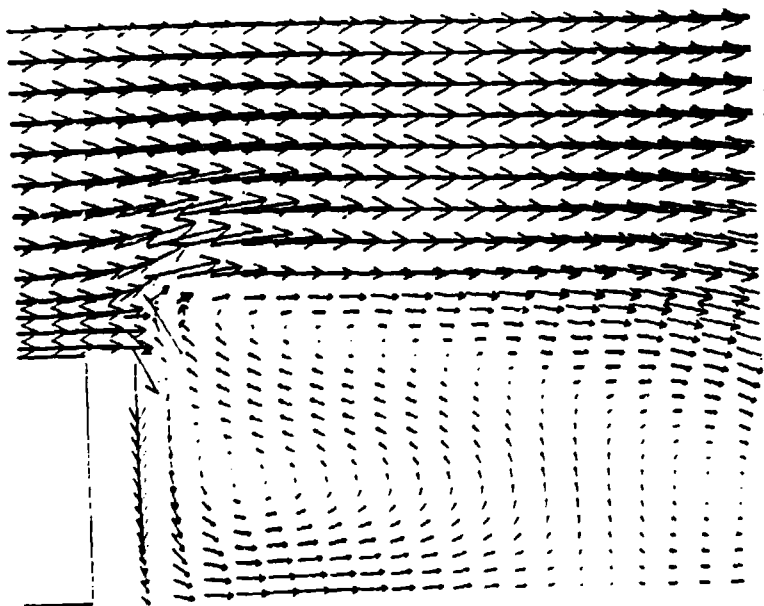


Figure 33. 50mm Deflector Slanted 30 Degrees; 0.0% Porosity, Bottom Edge 30mm Offset Downstream



(a)



(b)

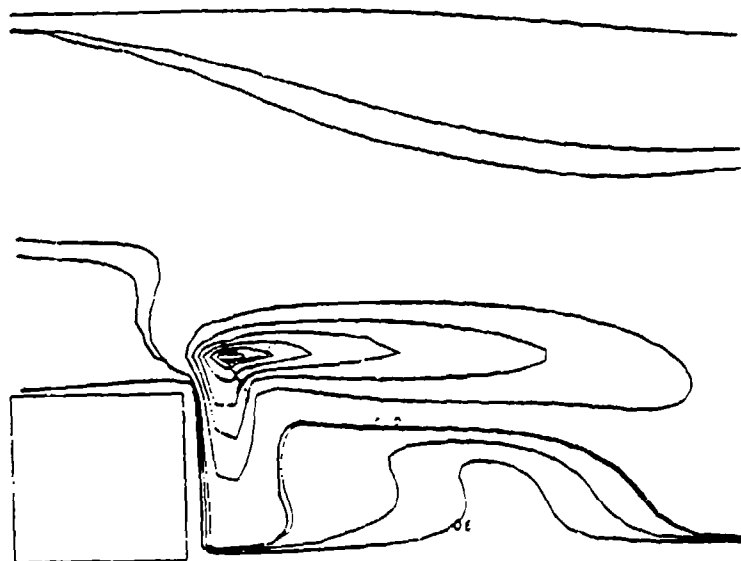
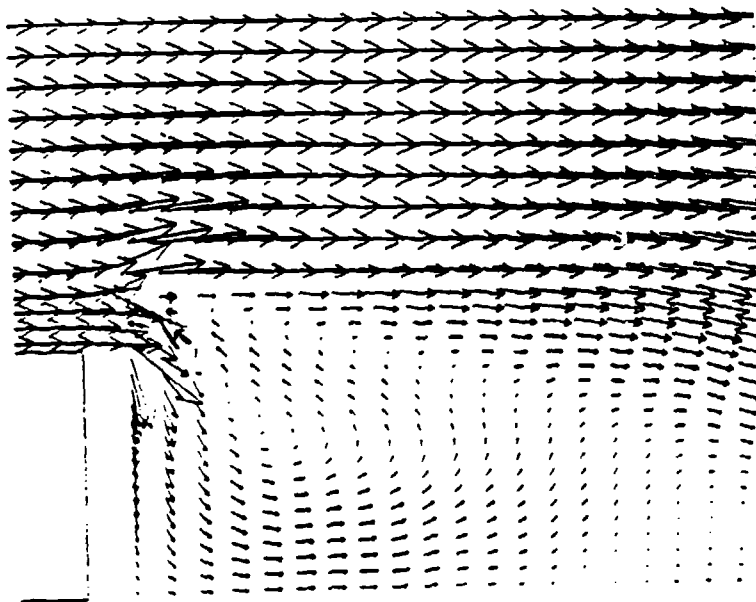


Figure 34. 50mm Deflector Slanted 30 Degrees; 5% Porosity, Bottom Edge 50mm Offset Downstream

(a)



(b)

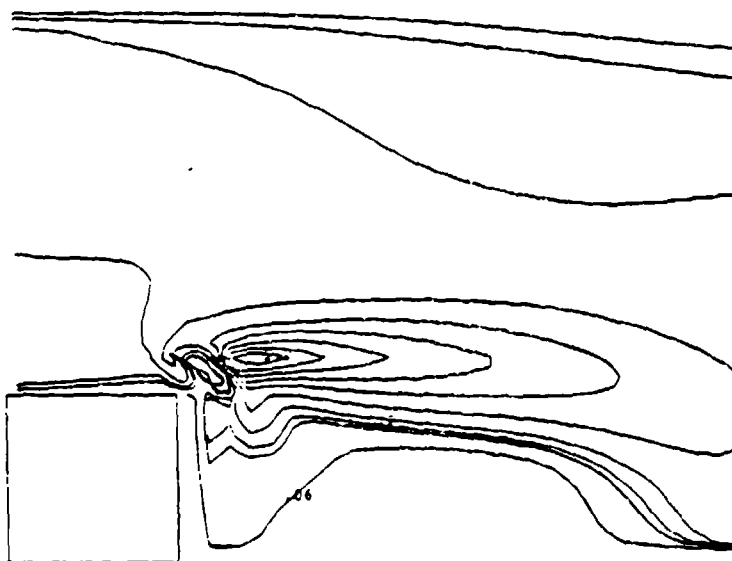


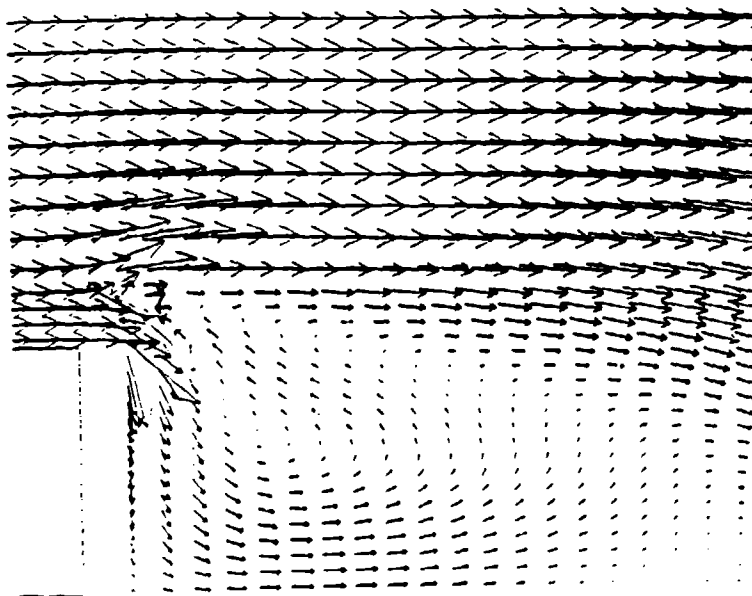
Figure 35. 50mm Cranked Deflector; 30/60 Degree, 0.0% Porosity, 50mm Offset Downstream

differed from the first in that the lower deflector was angled at 45 degrees to the vertical, as shown in Figure 36a and 36b.

Both configurations, however, gave quite similar results. Both had the primary recirculation zones shifted downstream with a strong "S" type flow located in the center of "the area of interest." Again, the TKE remained at approximately the same magnitude as found in the BFS.

Different porosities were tried but the iterations were interrupted each time by a numerical overflow. It was obvious that the automatic relaxation features built into "Phoenix" were not capable of dealing with this level of complexity.

(a)



(b)

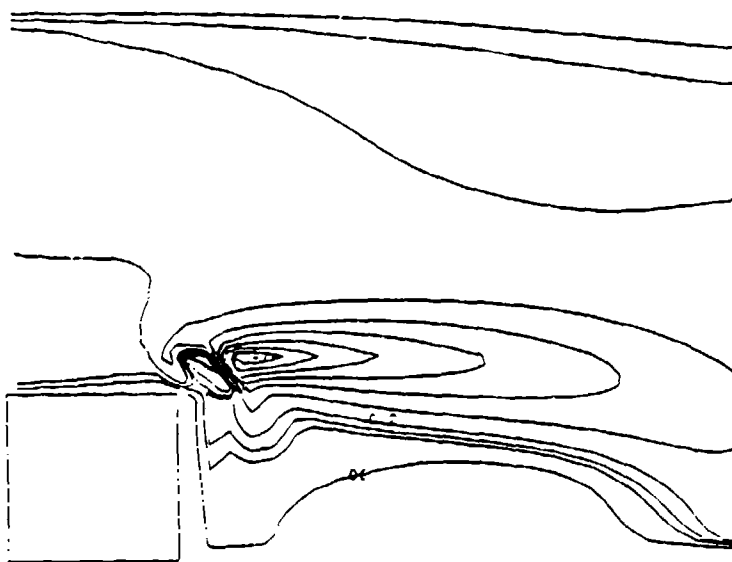


Figure 36. 50mm Cranked Deflector; 45/60 Degree, 0.0% Porosity, 50mm Offset Downstream

## V. CONCLUSIONS AND RECOMMENDATIONS

The results of this study show that a 50mm, 5% porous vertical deflector, whose lower edge is 25mm downstream of, and 12.5mm above the upper corner of the step, provided the best overall reduction of those deflectors tested, in velocity and turbulent kinetic energy for a 125mm high backward facing step. The velocity has been reduced on an average of 50% to 70% and the turbulent kinetic energy has been reduced upwards to 300%.

The porosity of the deflectors appears to be an independent parameter and therefore no one recommendation can be made. Each deflector position appears to require a unique porosity to achieve the best possible airflow.

It is also clear that incorrect deflector placement or orientation can do more harm than good by actually increasing both the velocities and the TKE.

Cranked deflectors, made of two attached straight segments, appear to be no improvement over single slanted segments.

Some recommendations for further studies are:

- (1) Attempt using as fine a grid as possible when setting up problems. This will take more computer time but give a more detailed and accurate representation of the flowfield.

- (2) Rerun the program for lower freestream velocities and compare the results with this present study's results to determine any relationships.
- (3) Use curvilinear Body Fitted Coordinates in "Phoenix" to set up curved type deflectors to learn more on the effect of deflector shape on airflow behavior.
- (4) Extend the study to 3-dimensional flow, i.e., study the influence of the airflow coming over the helicopter deck from around the sides of the hangar and especially from over the sides of the ship.

Complex flow problems that result in numerical overflow errors will require adjusting the "relaxation factors" in the "Phoenix" code so that convergence can occur.

# APPENDIX

## SAMPLE 01 FILE

TALK=T;RUN(1,1);VDU=1

\*\*\*\*\*

\*

\* GROUP 1. Run title and other preliminaries.

\*

TEXT( Slanted Deflector )

\*

\*\*\*\*\*

\*

\* GROUP 2. Transience; time-step specification.

\*

\*

\*\*\*\*\*

\*

\* GROUP 3. X-direction grid specification.

\*

\* Cartesian Grid Selected

CARTES=T

\* Extent of the Domain in the X-Direction: 1.276E+00

\* Number of Cells in the X-Direction

NX=29

\* Equal Grid Spacing in Subregion 1

\* SUBGRD(X,1,8, 3.520E-01, 1.000E+00)

INTEGER(NXF01,NXL01); NXF01=1; NXL01=8

XFRAC(1)= 4.400E-02;XFRAC(2)= 8.800E-02

XFRAC(3)= 1.320E-01;XFRAC(4)= 1.760E-01

XFRAC(5)= 2.200E-01;XFRAC(6)= 2.640E-01

XFRAC(7)= 3.080E-01;XFRAC(8)= 3.520E-01

\* Equal Grid Spacing in Subregion 2

\* SUBGRD(X,9,10, 8.800E-02, 1.000E+00)

INTEGER(NXF02,NXL02); NXF02=9; NXL02=10

XFRAC(9)= 3.960E-01;XFRAC(10)= 4.400E-01

\* Equal Grid Spacing in Subregion 3

\* SUBGRD(X,11,11, 4.400E-02, 1.000E+00)

INTEGER(NXF03,NXL03); NXF03=11; NXL03=11

XFRAC(11)= 4.840E-01

\* Equal Grid Spacing in Subregion 4

\* SUBGRD(X,12,29, 7.920E-01, 1.000E+00)

INTEGER(NXF04,NXL04); NXF04=12; NXL04=29

XFRAC(12)= 5.280E-01;XFRAC(13)= 5.720E-01

XFRAC(14)= 6.160E-01;XFRAC(15)= 6.600E-01

XFRAC(16)= 7.040E-01;XFRAC(17)= 7.480E-01

XFRAC(18)= 7.920E-01;XFRAC(19)= 8.360E-01

```

XFRAC(20)= 8.800E-01;XFRAC(21)= 9.240E-01
XFRAC(22)= 9.680E-01;XFRAC(23)= 1.012E+00
XFRAC(24)= 1.056E+00;XFRAC(25)= 1.100E+00
XFRAC(26)= 1.144E+00;XFRAC(27)= 1.188E+00
XFRAC(28)= 1.232E+00;XFRAC(29)= 1.276E+00

```

```

*
*****

```

```

*   GROUP 4. Y-direction grid specification.

```

```

*   Extent of the Domain in the Y-Direction:  1.276E+00

```

```

*   Number of Cells in the Y-Direction

```

```

NY=29

```

```

*   Equal Grid Spacing in Subregion 1

```

```

*   SUBGRD(Y,1,3, 1.320E-01, 1.000E+00)

```

```

INTEGER(NYF01,NYL01); NYF01=1; NYL01=3

```

```

YFRAC(1)= 4.400E-02;YFRAC(2)= 8.800E-02

```

```

YFRAC(3)= 1.320E-01

```

```

*   Equal Grid Spacing in Subregion 2

```

```

*   SUBGRD(Y,4,4, 4.400E-02, 1.000E+00)

```

```

INTEGER(NYF02,NYL02); NYF02=4; NYL02=4

```

```

YFRAC(4)= 1.760E-01

```

```

*   Equal Grid Spacing in Subregion 3

```

```

*   SUBGRD(Y,5,5, 4.400E-02, 1.000E+00)

```

```

INTEGER(NYF03,NYL03); NYF03=5; NYL03=5

```

```

YFRAC(5)= 2.200E-01

```

```

*   Equal Grid Spacing in Subregion 4

```

```

*   SUBGRD(Y,6,6, 4.400E-02, 1.000E+00)

```

```

INTEGER(NYF04,NYL04); NYF04=6; NYL04=6

```

```

YFRAC(6)= 2.640E-01

```

```

*   Equal Grid Spacing in Subregion 5

```

```

*   SUBGRD(Y,7,7, 4.400E-02, 1.000E+00)

```

```

INTEGER(NYF05,NYL05); NYF05=7; NYL05=7

```

```

YFRAC(7)= 3.080E-01

```

```

*   Equal Grid Spacing in Subregion 6

```

```

*   SUBGRD(Y,8,9, 8.800E-02, 1.000E+00)

```

```

INTEGER(NYF06,NYL06); NYF06=8; NYL06=9

```

```

YFRAC(8)= 3.520E-01;YFRAC(9)= 3.960E-01

```

```

*   Equal Grid Spacing in Subregion 7

```

```

*   SUBGRD(Y,10,11, 8.800E-02, 1.000E+00)

```

```

INTEGER(NYF07,NYL07); NYF07=10; NYL07=11

```

```

YFRAC(10)= 4.400E-01;YFRAC(11)= 4.840E-01

```

```

*   Equal Grid Spacing in Subregion 8

```

```

*   SUBGRD(Y,12,14, 1.320E-01, 1.000E+00)

```

```

INTEGER(NYF08,NYL08); NYF08=12; NYL08=14

```

```

YFRAC(12)= 5.280E-01;YFRAC(13)= 5.720E-01

```

```

YFRAC(14)= 6.160E-01

```

```

*   Equal Grid Spacing in Subregion 9

```

```

*   SUBGRD(Y,15,29, 6.600E-01, 1.000E+00)

```

```

INTEGER(NYF09,NYL09); NYF09=15; NYL09=29

```

```

YFRAC(15)= 6.600E-01;YFRAC(16)= 7.040E-01

```



YFRAC(17)= 7.480E-01;YFRAC(18)= 7.920E-01  
 YFRAC(19)= 8.360E-01;YFRAC(20)= 8.800E-01  
 YFRAC(21)= 9.240E-01;YFRAC(22)= 9.680E-01  
 YFRAC(23)= 1.012E+00;YFRAC(24)= 1.056E+00  
 YFRAC(25)= 1.100E+00;YFRAC(26)= 1.144E+00  
 YFRAC(27)= 1.188E+00;YFRAC(28)= 1.232E+00  
 YFRAC(29)= 1.276E+00

\*\*\*\*\*

\*

\* GROUP 5. Z-direction grid specification.

\*

\*

\*\*\*\*\*

\*

\* GROUP 6. Body-fitted coordinates or grid distortion.

BFC=T

SETPT(1,1,1,0,0,0)

SETPT(1,11,1,0,.22,0)

SETPT(59,11,1,1.276,.22,0)

SETPT(59,1,1,1.276,0,0)

DOMAIN(1,59,1,1,1,1)

SETLIN(XC,XF+LNI\*(XL-XF))

SETLIN(YC,YF)

SETLIN(ZC,ZF)

DOMAIN(1,1,1,11,1,1)

SETLIN(XC,XF)

SETLIN(YC,YF+LNJ\*(YL-YF))

SETLIN(ZC,ZF)

DOMAIN(1,59,11,11,1,1)

SETLIN(XC,XF+LNI\*(XL-XF))

SETLIN(YC,YF)

SETLIN(ZC,ZF)

DOMAIN(59,59,1,11,1,1)

SETLIN(XC,XF)

SETLIN(YC,YF+LNJ\*(YL-YF))

SETLIN(ZC,ZF)

DOMAIN(1,59,1,11,1,1)

MAGIC(T)

SETPT(1,15,1,0,.308,0)

SETPT(59,15,1,1.276,.308,0)

SETPT(21,15,1,.415,.308,0)

DOMAIN(1,1,11,15,1,1)

SETLIN(XC,XF)

SETLIN(YC,YF+LNJ\*(YL-YF))

SETLIN(ZC,ZF)

DOMAIN(59,59,11,15,1,1)

SETLIN(XC,XF)

SETLIN(YC,YF+LNJ\*(YL-YF))

SETLIN(ZC,ZF)

DOMAIN(1,21,15,15,1,1)

```

SETLIN(XC,XF+LNI*(XL-XF))
SETLIN(YC,YF)
SETLIN(ZC,ZF)
DOMAIN(21,59,15,15,1,1)
SETLIN(XC,XF+LNI*(XL-XF))
SETLIN(YC,YF)
SETLIN(ZC,ZF)
DOMAIN(21,21,11,15,1,1)
SETLIN(XC,XF+LNJ*(XL-XF))
SETLIN(YC,YF+LNJ*(YL-YF))
SETLIN(ZC,ZF)
DOMAIN(1,21,11,15,1,1)
MAGIC(T)
DOMAIN(21,59,11,15,1,1)
MAGIC(T)
SETPT(1,59,1,0,1.276,0)
SETPT(59,59,1,1.276,1.276,0)
DOMAIN(1,1,15,59,1,1)
SETLIN(XC,XF)
SETLIN(YC,YF+LNJ*(YL-YF))
SETLIN(ZC,ZF)
DOMAIN(1,59,59,59,1,1)
SETLIN(XC,XF+LNI*(XL-XF))
SETLIN(YC,YF)
SETLIN(ZC,ZF)
DOMAIN(59,59,15,59,1,1)
SETLIN(XC,XF)
SETLIN(YC,YF+LNJ*(YL-YF))
SETLIN(ZC,ZF)
DOMAIN(1,59,15,59,1,1)
MAGIC(T)
*
*
*****
*
*   GROUP 7. Variables stored, solved & named.
*
*   Solve for the PRESSURE
*   (Slab-by-Slab Method) *   (Arithmetic Averaging)
SOLVE(P1)
*   Solve for the X-DIRECTION VELOCITY COMPONENT
*   (Slab-by-Slab Method) *   (Arithmetic Averaging)
SOLVE(U1)
*   Solve for the Y-DIRECTION VELOCITY COMPONENT
*   (Slab-by-Slab Method) *   (Arithmetic Averaging)
SOLVE(V1)
*

```

```

*****
*
*  GROUP 8. Terms (in differential equations) & devices.
*
*****
*
*  GROUP 9. Properties of the medium (or media).
*
*  Set First-Phase Density Value
RH01= 1.100E+00
*  Set Laminar Kinematic Viscosity Value
ENUL= 1.000E-04
*  Select K-E Turbulen Model
*  ENUT = CMU * (Mixing Length) * K**0.5
*  EL1 = (CD * K**1.5)/E
TURMOD(KEMODL)
*
*****
*
*  GROUP 10. Inter-phase-transfer processes and properties.
*
*****
*
*  GROUP 11. Initialization of variable or porosity fields.
*
*  Initialize the X-DIRECTION VELOCITY COMPONENT
FIINIT(U1)= 2.400E+00
*  Initialize the TURBULENT KINETIC ENERGY
FIINIT(KE)= 2.060E-01
*  Initialize the KINETIC-ENERGY DISSIPATION RATE
FIINIT(EP)= 1.230E-01
*  Obstructed Region, Number 1
CONPOR(0.0,west,-NXF03,-NXL03,-NYF04,-NYL05,1,1)
*  Obstructed Region, Number 2
CONPOR(0.0,cell,-NXF01,-NXL01,-NYF01,-NYL03,1,1)
*
*****
*
*  GROUP 12. Convection and diffusion adjustments.
*
*****
*
*  GROUP 13. Boundary conditions and special sources.
*
*  INLET Boundary Condition, Named A
PATCH(A,west,NXF01,NXF01,NYF04,NYL04,1,1,1,1)
COVAL(A,P1,FIIFIU,RH01* 2.360E+00)
COVAL(A,U1,C1,YNS, 2.360E+00)

```

```

COVAL(A,V1,ONLYMS, 0.000E+00)
COVAL(A,KE,ONLYMS, 1.880E-01)
COVAL(A,EP,ONLYMS, 1.070E-01)
  * INLET Boundary Condition, Named C
PATCH(C,WEST,NXF01,NXF01,NYF05,NYL05,1,1,1,1)
COVAL(C,P1,FIXFLU,RHO1* 2.470E+00)
COVAL(C,U1,ONLYMS, 2.470E+00)
COVAL(C,V1,ONLYMS, 0.000E+00)
COVAL(C,KE,ONLYMS, 2.060E-01)
COVAL(C,EP,ONLYMS, 1.230E-01)
  * INLET Boundary Condition, Named D
PATCH(D,WEST,NXF01,NXF01,NYF06,NYL07,1,1,1,1)
COVAL(D,P1,FIXFLU,RHO1* 2.560E+00)
COVAL(D,U1,ONLYMS, 2.560E+00)
COVAL(D,V1,ONLYMS, 0.000E+00)
COVAL(D,KE,ONLYMS, 2.210E-01)
COVAL(D,EP,ONLYMS, 1.370E-01)
  * INLET Boundary Condition, Named E
PATCH(E,WEST,NXF01,NXF01,NYF08,NYL09,1,1,1,1)
COVAL(E,P1,FIXFLU,RHO1* 2.560E+00)
COVAL(E,U1,ONLYMS, 2.560E+00)
COVAL(E,V1,ONLYMS, 0.000E+00)
COVAL(E,KE,ONLYMS, 2.210E-01)
COVAL(E,EP,ONLYMS, 1.370E-01)
  * OUTLET Boundary Condition, Named OUTLET
PATCH(OUTLET,EAST,NXL04,NXL04,NYF01,NYL09,1,1,1,1)
COVAL(OUTLET,P1,FXP, 0.000E+00)
COVAL(OUTLET,KE,ONLYMS, 0.000E+00)
COVAL(OUTLET,EP,ONLYMS, 0.000E+00)
  * WALL Boundary Condition, Named TOPWALL
PATCH(TOPWALL,NWALL,NXF01,NXL04,NYL09,NYL09,1,1,1,1)
COVAL(TOPWALL,U1,GRND2, 0.000E+00)
COVAL(TOPWALL,KE,GRND2,GRND2)
COVAL(TOPWALL,EP,GRND2,GRND2)
  * WALL Boundary Condition, Named STEPWALL1
PATCH(STEPWALL1,NWALL,NXF01,NXL01,NYL03,NYL03,1,1,1,1)
COVAL(STEPWALL1,U1,GRND2, 0.000E+00)
COVAL(STEPWALL1,KE,GRND2,GRND2)
COVAL(STEPWALL1,EP,GRND2,GRND2)
  * WALL Boundary Condition, Named STEPWALL2
PATCH(STEPWALL2,EWALL,NXL01,NXL01,NYF01,NYL03,1,1,1,1)
COVAL(STEPWALL2,V1,GRND2, 0.000E+00)
COVAL(STEPWALL2,KE,GRND2,GRND2)
COVAL(STEPWALL2,EP,GRND2,GRND2)
  * WALL Boundary Condition, Named BOTWALL
PATCH(BOTWALL,SWALL,NXFC2,NXL04,NYF01,NYF01,1,1,1,1)
COVAL(BOTWALL,U1,GRND2, 0.000E+00)
COVAL(BOTWALL,KE,GRND2,GRND2)
COVAL(BOTWALL,EP,GRND2,GRND2)
  *

```

```

*****
*
*   GROUP 14. Downstream pressure for PARAB=.TRUE..
*
*
*****
*
*   GROUP 15. Termination of sweeps.
*
*   Number of Iterative Sweeps (Outer Iterations)
LSWEEP=600
*   Reference Residual for the PRESSURE
RESREF(P1)= 1.000E-04
*   Reference Residual for the X-DIRECTION VELOCITY
COMPONENT
RESREF(U1)= 1.000E-04
*   Reference Residual for the Y-DIRECTION VELOCITY
COMPONENT
RESREF(V1)= 1.000E-04
*   Reference Residual for the TURBULENT KINETIC ENERGY
RESREF(KE)= 1.000E-04
*   Reference Residual for the KINETIC-ENERGY DISSIPATION
RATE
RESREF(EP)= 1.000E-04
*
*****
*
*   GROUP 16. Termination of iterations.
*
*
*****
*
*   GROUP 17. Under-relaxation devices.
*
*   Automatic False-Time-Step Relaxation Applied to U1
REAL(SCALEL,SCALEU);SCALEL= 4.400E-02;SCALEU= 2.560E+00
RELAX(U1,FALSDT, 1.500E+00*SCALEL/SCALEU)
*   Automatic False-Time-Step Relaxation Applied to V1
RELAX(V1,FALSDT, 1.500E+00*SCALEL/SCALEU)
*   Automatic False-Time-Step Relaxation Applied to KE
RELAX(KE,FALSDT, 1.600E+00*SCALEL/SCALEU)
*   Automatic False-Time-Step Relaxation Applied to EP
RELAX(EP,FALSDT, 1.600E+00*SCALEL/SCALEU)
*

```

```

*****
*
*  GROUP 18. Limits on variables or increments to them.
*
*****
*
*  GROUP 19. Data communicated by satellite to GROUND.
*
*****
*
*  GROUP 20. Preliminary print-out.
*
*  Deactivate Print-Out of Satellite Data.
ECHO=F
*
*****
*
*  GROUP 21. Print-out of variables.
*
*  Printout for the PRESSURE
OUTPUT(P1,Y,N,N,Y,Y,Y)
*  Printout for the X-DIRECTION VELOCITY COMPONENT
OUTPUT(U1,Y,N,N,Y,Y,Y)
*  Printout for the Y-DIRECTION VELOCITY COMPONENT
OUTPUT(V1,Y,N,N,Y,N,N)
*  Printout for the TURBULENT KINETIC ENERGY
OUTPUT(KE,Y,N,N,Y,Y,Y)
*  Printout for the KINETIC-ENERGY DISSIPATION RATE
OUTPUT(EP,Y,N,N,Y,Y,Y)
*
*****
*
*  GROUP 22. Spot-value print-out.
*
*  X-Direction Index of Spot-Value
IXMON=6
*  Y-Direction Index of Spot-Value
IYMON=3
*
*****
*
*  GROUP 23. Field print-out and plot control.
*
*  Print TABLES AND PLOTS of Spot-Values and Residuals
ITABL=3
*

```

```
*****
*
*  GROUP 24. Preparations for continuation runs.
*
*  Save the Final Flow Field in a RE-START File
SAVE=T; NSAVE=CHAM
*
*****
STOP
```

### LIST OF REFERENCES

1. Naval Air Engineering Center NAEC-ENG-7526 Rev AF, Shipboard Aviation Facilities Resume, Department of the Navy, Naval Air Engineering Center, Lakehurst, New Jersey, April 1988, p. 122.
2. Naval Warfare Publication (NWP-42 Rev.H), Shipboard Helicopter Operating Procedures, Washington, D.C., Department of the Navy, March 1988.
3. Boeing Vertol Company Inter Office Memorandum, 107/H-46 Tunnel Strike Mishap History, April 1983.
4. Naval Air Test Center Technical Report, H-46 Dynamic Interface Tests Aboard the USS Missouri (BB63), Department of the Navy Naval Air Test Center, Patuxent River, Maryland, September, 1988, p. 7.
5. Madey, S.L. and L.D. Whitmer, SH-2F/SH-3F Interface Tests Aboard the USS Ticonderoga (CG 47), Naval Air Test Center Report No. RW-14R-83, November 1984.
6. Healey, J. Val., "Simulating the Helicopter/Ship Interface as an Alternative to Current Methods of Determining Safe Operating Envelopes," Naval Postgraduate School Report, NPS 67-86-003, Monterey, California, September 1986.
7. Johns, M. K., Flow Visualization of the Airwake Around a Model of a DD-963 Class Destroyer in a Simulated Atmospheric Boundary Layer, M.S. Thesis, Naval Postgraduate School, Monterey, California, September 1988.
8. Hunt, J.C.R., C.J. Abell, J.A. Peterka and H. Woo, "Kinematic Studies of the Flows around Free or Surface Mounted Obstacles; Applying Topology to Flow Visualization," Journal of Fluid Mechanics, Vol. 86, 1978, pp. 179, 200.
9. Bearman, P.W., "Vortex Shedding from Bluff Bodies," Annual Review of Fluid Mechanics, Vol. 16, 1984, pp. 195, 222.
10. Peterka, J.A., R.N. Meroney and K.M. Kothari, "Wind Flows About Buildings," Journal of Wind Engineering and Industrial Aerodynamics, Vol. 21, 1985, pp. 21-38.



11. Woo, H.G.C., J.A. Peterka, and J.E. Cermak, "Wind Tunnel Measurements in the Wakes of Structures," NASA Contractor Report, NASA CR-2806, 1977.
12. K.M. Kothari, J.A. Peterka and R.N. Meroney, "Stably Stratified Building Wakes," U.S. NRC Report, NUREG/CR-1247, 1979.
13. Eaton, J.K. and J.P. Johnston, "A Review of Research on Subsonic Turbulent Flow Reattachment," American Institute of Aeronautics and Astronautics, 80-1438, 1980, pp. 1093-1099.
14. Bradshaw, P. and F.Y. Wong, "The Reattachment and Relaxation of a Turbulent Shear Layer," Journal of Fluid Mechanics, Vol. 52, 1972, pp. 113-135.
15. Goldstein, R.J., V.L. Eriksen and E.R. Eckert, "Laminar Separation, Reattachment, and Transition of Flow over a Downstream-Facing-Step," Transactions of the ASME, Journal of Basic Engineering, Vol. 92D, No. 4, 1970, pp. 732-741.
16. Eaton, J.K. and J.P. Johnston, "Turbulent Flow Reattachment: An Experimental Study of the Flow and Structure behind a Backward-Facing Step," Department of Mechanical Engineering, Stanford University, Rept. MD-37, 1978.
17. Atli, V., "Subsonic Flow Over a Two-Dimensional Obstacle Immersed in a Turbulent Boundary Layer on a Flat Surface," Journal of Wind Engineering and Industrial Aerodynamics, Vol. 31, 1988, pp. 225-239.
18. Sinha, S.N., and A.K. Gupta, "Laminar Separating Flow Over Backsteps and Cavities," American Institute of Aeronautics and Astronautics, Vol. 20, 1982, pp. 370-375.
19. World Meteorological Organization, Technical Note No. 59, "Windbreaks and Shelterbelts," Geneva, Switzerland, 1964.
20. Perera, M.D.A.E.S., "Shelter Behind Two-Dimensional Solid and Porous Fences," Journal of Wind Engineering and Industrial Aerodynamics, Vol. 8, 1981, pp. 93-104.
21. Gandemer, J., "The Aerodynamic Characteristics of Windbreaks, Resulting in Empirical Design Rules," Journal of Wind Engineering and Industrial Aerodynamics, Vol. 7, 1981, pp. 15-36.
22. Spalding, B.D., The Phoenix Beginner's Guide, CHAM TR/100, Huntsville, Alabama, September 1989.

23. Plate, E.J., Engineering Meteorology, Elsevier Scientific Publishing Company, 1982.
24. Murakami, S. and A. Mochida, "3-D Numerical Simulation of Airflow Around a Cubic Model by Means of the Model," Journal of Wind Engineering and Industrial Aerodynamics, Vol. 31, 1988, pp. 283-303.
25. Yeung, P.K. and S.C. Kot, "Computation of Turbulent Flows Past Arbitrary Two-Dimensional Surface-Mounted Obstructions," Journal of Wind Engineering and Industrial Aerodynamics, Vol. 18, 1985, pp. 177-190.

### INITIAL DISTRIBUTION LIST

	No. Copies
1. Defenese Technical Information Center Cameron Station Alexandria, Virginia 22304-6145	2
2. Library, Code 50 Naval Postgraduate School Monterey, California 93943-5002	2
3. Department Chairman, Code AA Department of Aeronautics and Astronautics Naval Postgraduate School Monterey, California 93943-5000	1
4. Commander Naval Air Systems Command Air Vehicle Division Attn: Mr. Jonah Ottensoser, Code Air 53011C Jefferson Plaza 2, Rm. 904 Washington, D.C. 20361	2
5. Mr. Bernard Ferrier CANDAIR LTD. 1800 Laurentieu Blvd. Saint Laurent Quebec, Canada H4R1KZ	1
6. Naval Air Test Center Attn: Mr. Dean Carico, Code RW40A Patuxent River, Maryland 20670	1
7. Naval Air Test Center Attn: Mr. Jerry Higman, Code RW81 Patuxent River, Maryland 20670	1
8. Dr. J. Val Healey, Code AA/He Department of Aeronautics and Astronautics Naval Postgraduate School Monterey, California 93943-5000	6
9. Dr. David Salinas, Code ME/Sa Department of Mechanical Engineering Naval Postgraduate School Monterey, California 93943-5000	1

10. Mr. Neil Gilbert 1  
Aeronautical Division  
Aeronautical Research Laboratories  
506 Lorimer Street  
Fisherman's Bend  
Box 4331 P.O.  
Melbourne, Victoria 3001  
Australia
11. Naval Air Test Center 1  
Code RW40, Attn: Kurt Long  
Patuxent River, Maryland 20670
12. Mr. Tony Cricelli, Code AA 1  
Department of Aeronautics and Astronautics  
Naval Postgraduate School  
Monterey, California 93943-5000
13. Lt. Scott G. Woolman 1  
1854 Marlow Place  
Crofton, Maryland 21114

**END  
FILMED**

DATE: 7-91

**DTIC**